

Consistency of hadronic vacuum polarization between lattice QCD and the R ratio

Christoph Lehner^{*}

*Universität Regensburg, Fakultät für Physik, 93040, Regensburg, Germany
and Physics Department, Brookhaven National Laboratory, Upton, New York 11973, USA*

Aaron S. Meyer[†]

Physics Department, Brookhaven National Laboratory, Upton, New York 11973, USA



(Received 15 March 2020; accepted 30 March 2020; published 23 April 2020)

There are emerging tensions for theory results of the hadronic vacuum polarization contribution to the muon anomalous magnetic moment both within recent lattice QCD calculations and between some lattice QCD calculations and R-ratio results. In this paper, we work toward scrutinizing critical aspects of these calculations. We focus in particular on a precise calculation of Euclidean position-space windows defined by RBC/UKQCD that are ideal quantities for cross-checks within the lattice community and with R-ratio results. We perform a lattice QCD calculation using physical up, down, strange, and charm sea quark gauge ensembles generated in the staggered formalism by the MILC Collaboration. We study the continuum limit using inverse lattice spacings from $a^{-1} \approx 1.6$ GeV to 3.5 GeV, identical to recent studies by FNAL/HPQCD/MILC and Aubin *et al.* and similar to the recent study of BMW. Our calculation exhibits a tension for the particularly interesting window result of $a_\mu^{\text{ud,conn.,isospin,W}}$ from 0.4 to 1.0 fm with previous results obtained with a different discretization of the vector current on the same gauge configurations. Our results may indicate a difficulty related to estimating uncertainties of the continuum extrapolation that deserves further attention. In this work, we also provide results for $a_\mu^{\text{ud,conn.,isospin}}$, $a_\mu^{\text{s,conn.,isospin}}$, $a_\mu^{\text{SIB,conn.}}$ for the total contribution and a large set of windows. For the total contribution, we find $a_\mu^{\text{HVPLO}} = 714(27)(13)10^{-10}$, $a_\mu^{\text{ud,conn.,isospin}} = 657(26)(12)10^{-10}$, $a_\mu^{\text{s,conn.,isospin}} = 52.83(22)(65)10^{-10}$, and $a_\mu^{\text{SIB,conn.}} = 9.0(0.8)(1.2)10^{-10}$, where the first uncertainty is statistical and the second systematic. We also comment on finite-volume corrections for the strong-isospin-breaking corrections.

DOI: 10.1103/PhysRevD.101.074515

I. INTRODUCTION

The established theory result for the muon anomalous magnetic moment, a_μ , exhibits a 3.3σ [1] to a 3.8σ [2] tension with the results of the BNL experiment [3]. Within this year, we expect the Fermilab $g - 2$ experiment [4] to release first results toward their target to reduce the uncertainties of the BNL experiment by a factor of 4. In the near future, we also look forward to results from the methodologically independent experimental program at J-PARC [5]. These results are highly anticipated and are accompanied by a concerted effort of the theory community to improve upon and scrutinize the existing standard model

results, most importantly for the hadronic vacuum polarization (HVP) [1,6–30] and hadronic light-by-light (HLbL) [31,32] contributions, which currently limit the precision of the theory result. The muon $g - 2$ theory Initiative, a multiyear community effort [33–37], is now in the final stages of writing a white paper summarizing the current theory status [38].

For the HLbL contribution, new analytic approaches [39–43] as well as the first *ab initio* lattice QCD calculation [32] building on multiyear methodology development [44–49] so far show consistent results and rule out the HLbL contribution as an explanation for the current tension between theory and experiment.

For the HVP contribution, however, tensions exist within lattice QCD calculations [50] as well as between lattice QCD calculations and R-ratio results [27,50]. At this point, the lattice calculations exhibiting a tension with R-ratio results share some aspects. They are performed at physical pion mass, with staggered sea quarks and a conserved valence vector current, and use inverse lattice spacings in the range from $a^{-1} \approx 1.6$ GeV to $a^{-1} \approx 3.5$ GeV. At the

^{*}christoph.lehner@ur.de

[†]ameyer@quark.phy.bnl.gov

Published by the American Physical Society under the terms of the [Creative Commons Attribution 4.0 International license](#). Further distribution of this work must maintain attribution to the author(s) and the published article's title, journal citation, and DOI. Funded by SCOAP³.

same time, a joint study of lattice QCD and R-ratio results performed by the RBC/UKQCD Collaboration [21] using domain-wall sea quarks at physical pion mass with $a^{-1} = 1.7$ to 2.4 GeV showed no significant tension.

Concretely, there are two tensions for the isospin-symmetric quark-connected light-quark contribution (Fig. 13). The first is for the Euclidean position-space window $a_{\mu}^{\text{ud,conn.,isospin,W}}$ for times $t_0 = 0.4$ fm, $t_1 = 1.0$ fm, and $\Delta = 0.15$ fm as defined by RBC/UKQCD [21] between Aubin *et al.* [50] on one side and RBC/UKQCD [21] and a combined R-ratio/lattice result [21,27,50] on the other side. The second is a tension between the total $a_{\mu}^{\text{ud,conn.,isospin}}$ with high values for BMW [27] and lower values for FNAL/HPQCD/MILC [24] and ETMC [30]. In this work, we focus on scrutinizing the first tension.

To this end, we use the same lattice QCD ensembles as Aubin *et al.* [50] but use a site-local current instead of a conserved current. Within this framework, we then consider different approaches toward the continuum limit for windows in the staggered formalism and provide an analysis with minimal input from effective theories. In our analysis, we find a substantially lower value for $a_{\mu}^{\text{ud,conn.,isospin,W}}$ compared to Ref. [50]. This is particularly noteworthy since the same sea-quark sector is used and may indicate difficulties with properly estimating uncertainties associated with the continuum limit.

Within our numerical framework, we can also access the connected strong-isospin-breaking contribution as well as the strange-quark connected contribution. We provide results also for these contributions including a wide range of different windows. We hope that these results will prove useful to further understand the current tensions.

This manuscript is organized as follows: Sec. II discusses the main methods used in the analysis, including the window method and a correlator smoothing technique to reduce the unwanted parity partner contributions. Section III gives information about the ensembles used for this study and the computational setup for our data generation. In Sec. IV, we describe our analysis and uncertainty estimates. In this section, we in particular also comment on finite-volume corrections to the strong-isospin-breaking contributions. In Sec. V, we summarize and give some concluding remarks. Appendix provides additional tables of results for cross-comparisons with other analyses.

II. METHODOLOGY

A. General setup

In this work, we perform a calculation of the HVP contribution to a_{μ} using the Euclidean time-momentum representation [51],

$$a_{\mu}^{\text{HVP}} = \sum_{t=0}^{\infty} w_t C(t), \quad (1)$$

with sum over Euclidean time t and

$$C(t) = \frac{1}{12\pi^2} \int_0^{\infty} d(\sqrt{s}) R(s) s e^{-\sqrt{s}t}, \quad (2)$$

with R-ratio $R(s) = (3s/4\pi\alpha^2)\sigma(s, e^+e^- \rightarrow \text{had})$. We can also relate $C(t)$ to vacuum expectation values of vector currents V_{μ} that we compute in lattice QCD + QED as

$$C(t) = \frac{1}{3} \sum_{i,\vec{x}} \langle V_i(\vec{x}, t) V_i(\vec{0}, 0) \rangle, \quad (3)$$

where the sum is over spatial indices i and all points \vec{x} in the spatial volume and

$$V_{\mu} = \frac{2}{3} i(\bar{u}\gamma_{\mu}u + \bar{c}\gamma_{\mu}c) - \frac{1}{3} i(\bar{d}\gamma_{\mu}d + \bar{s}\gamma_{\mu}s + \bar{b}\gamma_{\mu}b), \quad (4)$$

with quark flavors u, d, s, c, b . In the absence of QED but the presence of a quark-mass splitting between up and down quarks with individual quark masses,

$$\begin{aligned} m_u &= m_l - \Delta m, \\ m_d &= m_l + \Delta m, \end{aligned} \quad (5)$$

the total up, down, and strange contributions can be written as

$$\begin{aligned} a_{\mu}^{\text{uds}} &= a_{\mu}^{\text{ud,conn.,isospin}} + a_{\mu}^{\text{s,conn.,isospin}} + a_{\mu}^{\text{uds,disc.,isospin}} \\ &\quad + a_{\mu}^{\text{SIB,conn.}} + a_{\mu}^{\text{SIB,disc.}}. \end{aligned} \quad (6)$$

In this work, we focus on the connected contributions $a_{\mu}^{\text{ud,conn.,isospin}}$, $a_{\mu}^{\text{s,conn.,isospin}}$, and $a_{\mu}^{\text{SIB,conn.}}$, which we express as

$$a_{\mu}^{\text{ud,conn.,isospin}} = 5a_{\mu}^v(m_l), \quad (7)$$

$$a_{\mu}^{\text{s,conn.,isospin}} = a_{\mu}^v(m_s), \quad (8)$$

where m_v denotes the mass of the valence quark and

$$a_{\mu}^v(m_v) = \frac{1}{9} c(m_v) \quad (9)$$

in terms of the diagrams of Fig. 1. The connected strong-isospin-breaking (SIB) contribution can be written as

$$\begin{aligned} a_{\mu}^{\text{SIB,conn.}} &= \frac{2}{3} \Delta M(m_v = m_l) \\ &= 3\lambda_0 \frac{\kappa - 1}{\kappa + 1} \lim_{\lambda \rightarrow \lambda_0} \frac{\partial}{\partial \lambda} a_{\mu}^v(\lambda = m_v/m_s), \end{aligned} \quad (10)$$

where diagrams M and O of Fig. 2 are related to diagrams c and d of Fig. 1 by

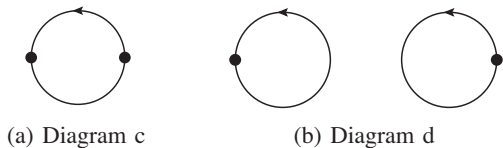


FIG. 1. Feynman diagrams for the isospin-symmetric contribution to the HVP. The dots represent the vector currents coupling to external photons. These diagrams represent gluon contributions to all orders.

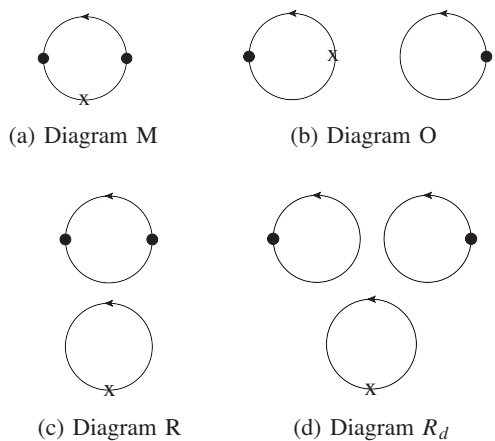


FIG. 2. Connected and disconnected strong-isospin-breaking (SIB) diagrams. The cross denotes the insertion of a scalar operator. Also here each diagram represents gluon contributions to all orders.

$$\frac{\partial}{\partial m_v} c(m_v) = -2M(m_v), \quad (11)$$

$$\frac{\partial}{\partial m_v} d(m_v) = -2O(m_v) \quad (12)$$

and

$$\lambda_0 \equiv \frac{m_l}{m_s}, \quad \kappa \equiv \frac{m_u}{m_d}. \quad (13)$$

Both κ and λ_0 are obtained from FLAG 2019 [52], where λ_0 is taken from $2 + 1 + 1$ flavor simulations and κ is from $2 + 1$ flavor simulations. Only one $2 + 1 + 1$ flavor result for κ is available, so we choose to use the $2 + 1$ flavor simulation so as not to tie our results to a single external measurement. The values for these quantities are

$$\kappa = 0.485(19), \quad \lambda_0^{-1} = 27.23(10). \quad (14)$$

The diagrams R and R_d do not contribute in the definition of the isospin-symmetric point given in Eq. (5).

The weighting kernel in Eq. (1) is determined as [51,53]

$$w_t^f = 8\alpha^2 m_\mu^2 \int_0^\infty ds K(s, m_\mu) f(t, \sqrt{s}), \quad (15)$$

$$K(s, m_\mu) = \frac{sZ(s, m_\mu)^3(1 - sZ(s, m_\mu))}{1 + m_\mu^2 s Z(s, m_\mu)^2}, \quad (16)$$

$$Z(s, m_\mu) = \frac{\sqrt{s^2 + 4m_\mu^2 s} - s}{2m_\mu^2 s}, \quad (17)$$

where we will use two alternative choices for the function f ,

$$f_p(t, q) = \frac{\cos(qt) - 1}{q^2} + \frac{1}{2} t^2, \quad (18)$$

$$f_{\hat{p}}(t, q) = \frac{\cos(qt) - 1}{(2 \sin(q/2))^2} + \frac{1}{2} t^2. \quad (19)$$

We refer to the choice $f = f_p$ as the p prescription and to the choice of $f = f_{\hat{p}}$ as the \hat{p} description. Both are well motivated within a lattice calculation and differ only due to discretization errors. We will provide results for both and scrutinize the difference when considering uncertainties associated with the continuum limit.

B. Window method

It is instructive to isolate specific ranges of Euclidean time in order to better understand their contributions to a_μ^v . This can be accomplished by constructing windows that suppress contributions outside of the window region [21]. Rather than using Heaviside step functions to isolate these ranges, which would have significant dependence on the lattice cutoff near the boundary of the window, a smoothed step is considered [16,51],

$$\Theta(t, \mu, \Delta) = [1 + \tanh[(t - \mu)/\Delta]]/2. \quad (20)$$

This step function suppresses all values below μ and has a width parametrized by Δ . From these step functions, windows into specific regions of a_μ^v Euclidean time can be studied by instead summing the integral relation

$$a_\mu^{v,W}(t_0, t_1, \Delta) = \sum_{t=0}^{\infty} w_t C(t) [\Theta(t, t_1, \Delta) - \Theta(t, t_0, \Delta)]. \quad (21)$$

We will quote results both for the total contribution, corresponding to $t_0 \rightarrow -\infty$ and $t_1 \rightarrow \infty$, as well as specific windows. It should be noted that windows of a_μ^v that isolate specific Euclidean distance scales can be related to specific windows of timelike s in the experimental data used in the R ratio [21].

C. Parity improvement

When performing computations with staggered quarks, parity projections are not possible and correlation functions receive contributions from parity partner states. These parity partners have different spin and taste quantum numbers and constitute unwanted contributions to the correlation function. The unwanted contributions come as oscillating terms with a prefactor proportional to $(-1)^{t/a}$. To suppress these contributions to the correlation functions, we also study the improved parity averaging (IPA) procedure which averages neighboring time slices [54],

$$C^{\text{IPA}}(t) = \frac{e^{-m_\rho t}}{4} \left[\frac{C(t-1)}{e^{-m_\rho(t-1)}} + 2 \frac{C(t)}{e^{-m_\rho t}} + \frac{C(t+1)}{e^{-m_\rho(t+1)}} \right]. \quad (22)$$

The correlation function times are weighted by exponential factors that reflect the falloff of the correlation function in order to better enforce the cancellation of oscillating parity partner contributions. The exponent used is the ρ meson mass, obtained from PDG [55], which is expected to give the best cancellation in the ρ resonance peak. The ρ resonance region accounts for the majority of the contribution to a_μ^ν , and so cancellation in this region would be most beneficial. In the continuum limit, the choice of m_ρ is irrelevant; however, the IPA prescription using the rho mass is not well motivated for very short or long distances or for heavier quark masses.

III. NUMERICAL SETUP

The computation in this work is performed with the highly improved staggered quark action for both valence and sea quarks. The ensembles were generated by the MILC Collaboration [56], and details about these ensembles are given in Table I. For the staggered quark action, the vector current operator is written as

$$V_i(x_4) = \sum_{\vec{x}} (-1)^{x_i/a} \epsilon(x) \bar{\chi}(\vec{x}, x_4) \chi(\vec{x}, x_4), \quad (23)$$

where $\chi(\vec{x}, x_4)$ is the staggered one-component spinor and $\epsilon(x)$ is the usual staggered sign phase,

$$\epsilon(x) = (-1)^{\sum_\mu x_\mu/a}. \quad (24)$$

TABLE I. List of ensemble parameters for ensembles used in this study. Table values reproduced from Table I of Ref. [24]. The gradient flow scale in the continuum, $w_0 = 0.1715(9)$ fm, taken from Eq. (18) of Ref. [57].

Ens	$L^3 \times T$	w_0/a	$Z_V(\bar{s}s)$	M_{π_S}	$M_\pi L$
48c	$48^3 \times 64$	1.41490(60)	0.99220(40)	132.73(70)	3.9
64c	$64^3 \times 96$	1.95180(70)	0.99400(50)	128.34(68)	3.7
96c	$96^3 \times 192$	3.0170(23)	0.9941(11)	134.95(72)	3.7

This vector current bilinear has the advantage of being local to a single site. Vector currents of other tastes may be formed by distributing the quark and antiquark over the unit hypercube, but these bilinear combinations require extra inversions and so were not explored.

Sources are inverted on random noise vectors that solve the Green's function equation,

$$\sum_y D_{xy}^{ab} G_{y;t}^{bc} = \eta_x^{ac} \delta_{x_0,t}, \quad (25)$$

with η satisfying the condition

$$\langle \eta_x^{ab} (\eta_y^{bc})^\dagger \rangle = \frac{1}{8} \delta^{ac} \delta_{xy} \prod_{i=1}^3 (1 - (-1)^{x_i/a}). \quad (26)$$

The phase factor on the rhs of Eq. (26) results from projecting out sites where x_i/a is odd for at least one i . When the propagator obtained from Eq. (25) is contracted with its Hermitian conjugate at the source, the construction produces an operator that couples to many staggered spin-taste meson irreducible representations. The vector current of Eq. (23) is contracted explicitly at the sink, projecting out the unwanted spin-taste irreps at the source and reproducing the correlation function of Eq. (3) up to a factor of 8. In the propagator solutions for the Dirac equation, the Naik epsilon term is set to zero.

Results are computed on three ensembles with $2+1+1$ flavors of sea quarks and up to seven choices of valence quark mass per ensemble. The parameters for the three ensembles used in this study are given in Table I. The sea quark masses are given in Table II along with retuned quark masses for the strange quarks. The valence quark masses used in this study are rational fractions λ times the tuned strange-quark masses from Table II. The list of rational fractions is given in Table III along with the number of time sources per configurations and the number of configurations used for each ensemble and mass combination.

IV. RESULTS

A. Bounding method

For the two lightest masses $\lambda = 1/12$ and $\lambda = 1/6$, we also employ the bounding method [20,21,60] to create strict

TABLE II. Sea and valence quark masses used for each ensemble. Sea quark masses are listed in Ref. [24]. Valence quark masses are taken as fractional ratios of the tuned strange-quark masses given in Table V of Ref. [56].

Ens	m_ℓ	m_s	m_c	$m_{s,\text{tuned}}$
48c	0.00184	0.0507	0.628	0.05252(10)
64c	0.00120	0.0363	0.432	0.03636(9)
96c	0.0008	0.022	0.260	0.02186(6)

TABLE III. Number of configurations and time sources used for each ensemble and valence quark mass combination. The valence quark masses are quoted as ratios of the valence quark mass to the tuned strange-quark mass, $\lambda \equiv m_{\text{valence}}/m_{s,\text{tuned}}$, obtained from Table II. The 64c $\lambda = 1/12$ mass point was inverted on double the number of time sources compared to the other 64c mass points, for a total of 48 time sources. This ensemble/mass point combination was computed using the truncated solver method [58] in an AMA setup [59] with 20 configurations solved with full precision and 1540 configurations solved with a residual of 10^{-4} . The 20 full-precision solves are used to correct the bias introduced by this procedure, which was tuned to have negligible impact on the results.

		$N_{\text{conf}}[\lambda]$						
Ens	$t_{\text{src}}/\text{Conf}$	1/1	3/4	2/3	1/2	1/3	1/6	1/12
48c	16	50	50	50	100	100	800	800
64c	24(48*)	32	32	32	64	64	192	20/1540*
96c	24	32	32

upper and lower bounds for a_μ^v . We show results for the total a_μ^v in Fig. 3. In the bounding method, one replaces the correlator $C(t)$ by

$$\tilde{C}(t; T, \tilde{E}) = \begin{cases} C(t) & t < T, \\ C(T)e^{-(t-T)\tilde{E}} & t \geq T, \end{cases} \quad (27)$$

which then defines a strict upper or lower bound of $C(t)$ for each t given an appropriate choice of \tilde{E} . For the upper bound, we use \tilde{E} equals to the free two-pion ground state energy and for the lower bound we use $\tilde{E} = \infty$ [21]. We select the data points of $T = T_0$, where upper and lower bounds agree. For $\lambda = 1/12$, we use $T_0/a = 21$ for the 48c ensemble and $T_0/a = 34$ for the 64c ensemble. For $\lambda = 1/6$, we use $T_0/a = 24$ for the 48c ensemble and $T_0/a = 36$ for the 64c ensemble.

B. Continuum extrapolation

The first part of the analysis consists of taking the continuum limit of each individual mass point. This extrapolation is applied before considering extrapolations in quark mass or volume.

Figures 4 and 5 show the extrapolation of the $m_v/m_s = 1/1$ and $1/3$ data to the continuum for both the unimproved and improved data. These mass points have data for all three ensembles and are used to study the continuum-extrapolation behavior of the windows. A linear extrapolation is performed on the 64c and 96c ensembles to obtain the continuum limit. A systematic uncertainty is obtained by taking the difference between the 48c and 64c extrapolation and the 64c and 96c extrapolation for both these mass points. We use the average of these systematic uncertainties for $\lambda = 1/1$ and $\lambda = 1/3$ as an additional systematic

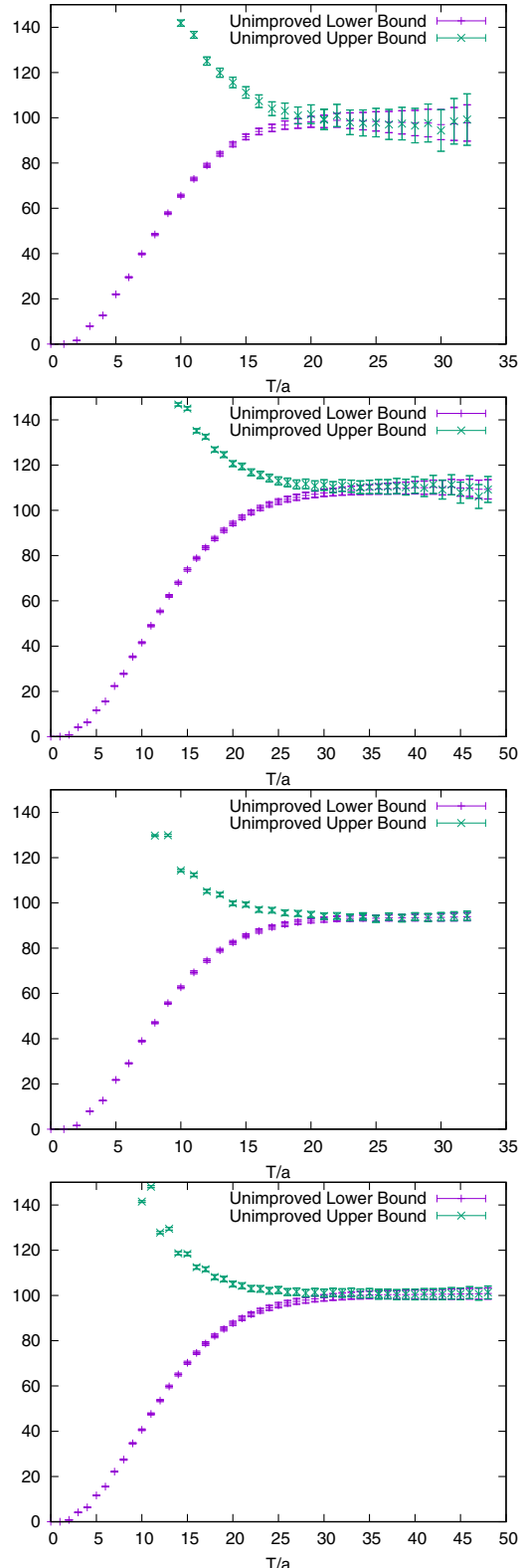


FIG. 3. We show $10^{10} a_\mu^{v,\text{BND}}(T)$ with $a_\mu^{v,\text{BND}}(T) = \sum_{t=0}^{\infty} w_t C(t, T, \tilde{E})$ for both the upper bound \tilde{E} equals to the free two-pion ground state energy as well as the lower bound $\tilde{E} = \infty$. From top to bottom, the results are for $\lambda = 1/12$ on the 48c ensemble, $\lambda = 1/12$ on the 64c ensemble, $\lambda = 1/6$ on the 48c ensemble, and $\lambda = 1/6$ on the 64c ensemble.

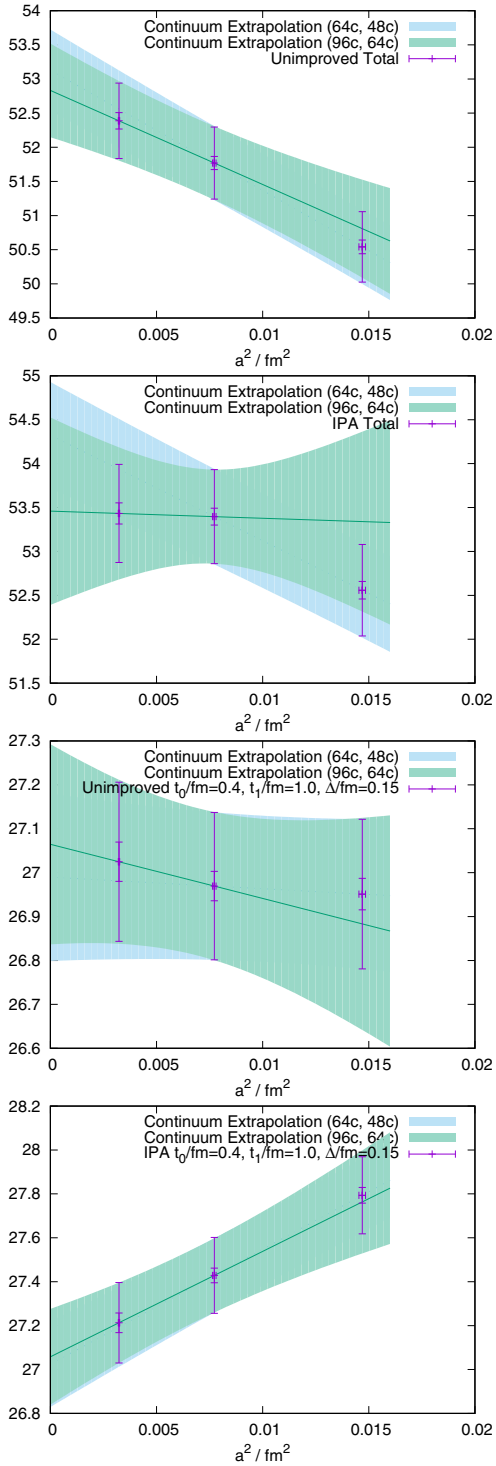


FIG. 4. Continuum extrapolation of the $m_v/m_s = 1/1$ data for both the total a_μ^v contribution and for the window with $(t_0, t_1) = (0.4, 1.0)$ fm. We show the unimproved data and as well as data with the parity improvement described in Sec. II C. The data include both statistical and systematic uncertainties. The extrapolations with either 48c and 64c or with 64c and 96c ensembles are shown as shaded bands.

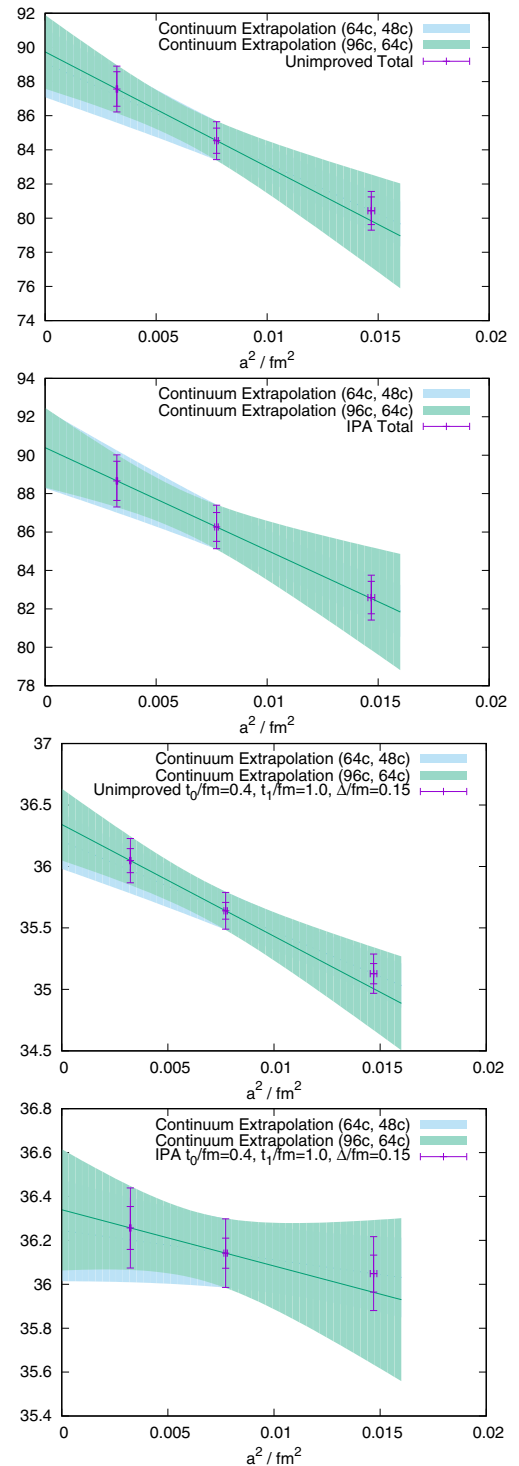


FIG. 5. Same as Fig. 4, but for $m_v/m_s = 1/3$.

uncertainty that we apply also to all other mass points, where there is no third ensemble.

Figures 6 and 7 show the continuum extrapolation for various choices of $t_1 - t_0 = 0.1$ fm windows for both unimproved and improved data. All of these windows

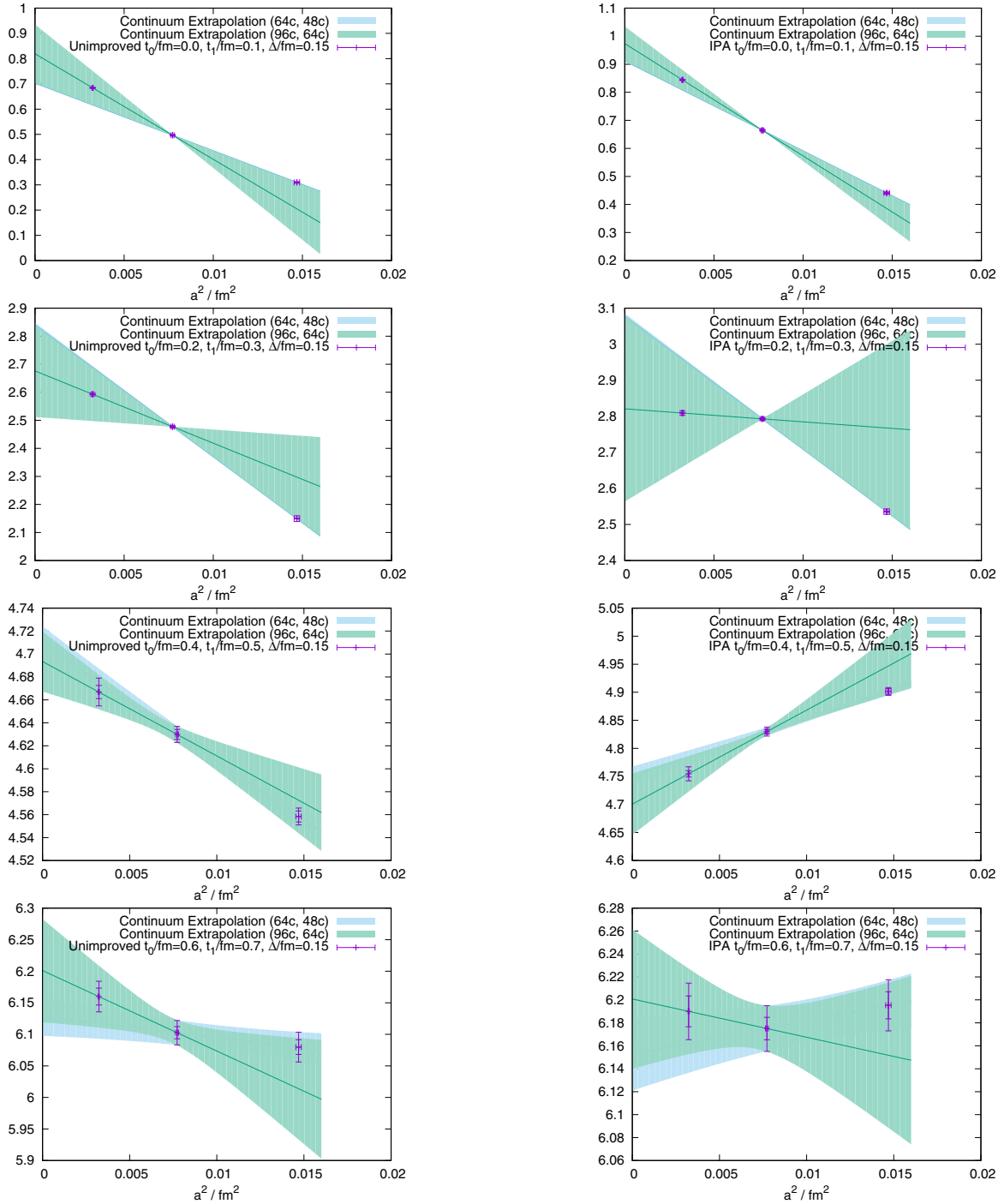


FIG. 6. Windows with $t_1 - t_0 = 0.1$ fm for the $m_v/m_s = 1/3$ valence mass. Windows with $t_{0,1} \leq 0.8$ fm are included. We notice a significant uncertainty in the continuum extrapolation, which we may attribute to the somewhat small difference between t_0 and t_1 . We therefore also show results for $t_1 - t_0 = 0.2$ fm in later tables. The left and right columns are for the unimproved data and for the data with the parity improvement, respectively. The parity improvement is only well motivated in the ρ resonance region and so is not expected to work well for shorter distances.

are shown for the $m_v/m_s = 1/3$ mass point. The continuum extrapolations for windows up to $t_0 = 0.8$ fm have visible contributions from discretization effects that are nonlinear in a^2 . Beyond $t_0 = 0.8$ fm, the windows have no resolvable nonlinear discretization effects and are

consistent well within statistical uncertainties for $t_0 \geq 1.0$ fm. The IPA is only well motivated in the region of the ρ resonance peak and has larger discretization effects for short-distance windows. In the long-distance windows, IPA becomes identical to the unimproved data.

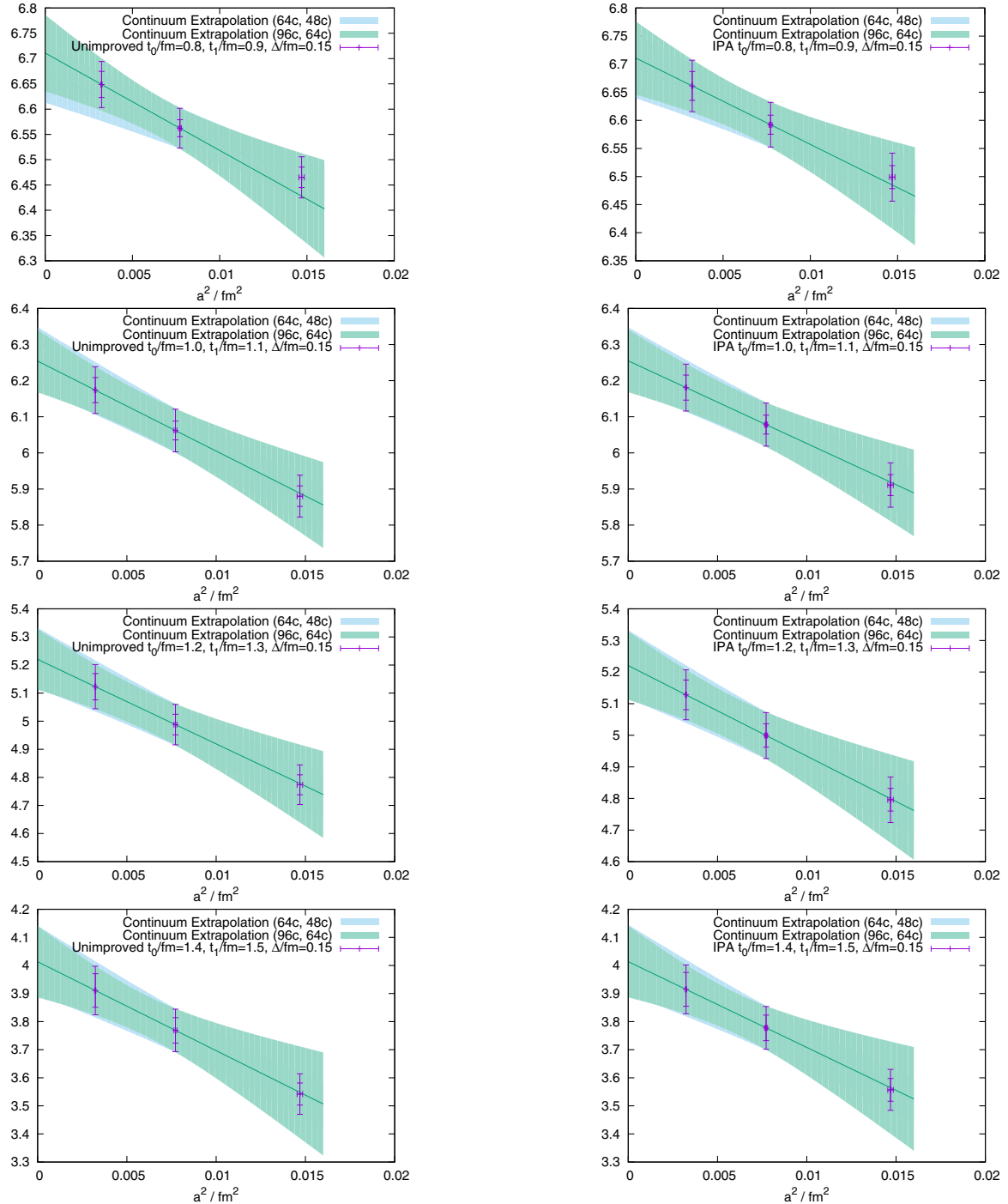


FIG. 7. Same as Fig. 6, but for windows with $t_{0,1} \geq 0.8$ fm. For long-distance windows, the continuum extrapolation is no longer an issue and fits are very consistent with data.

Figure 8 demonstrates the effect of the window smearing parameter Δ on the continuum extrapolation. If Δ is smaller than the lattice spacing, the window turns on or off rapidly and can resolve contributions from individual time slices. These discretization effects are clearly visible for the coarsest ensembles when Δ is too small. This is cleaned up by increasing the window smearing. The IPA also

smears neighboring time slices, which reduces the effect of discretizations for even the smallest window smearings.

Figure 9 shows the difference between the IPA procedure of Eq. (22) and the unimproved total result for several choices of valence quark mass and lattice spacing. The improvement with the ρ resonance mass in Eq. (22)

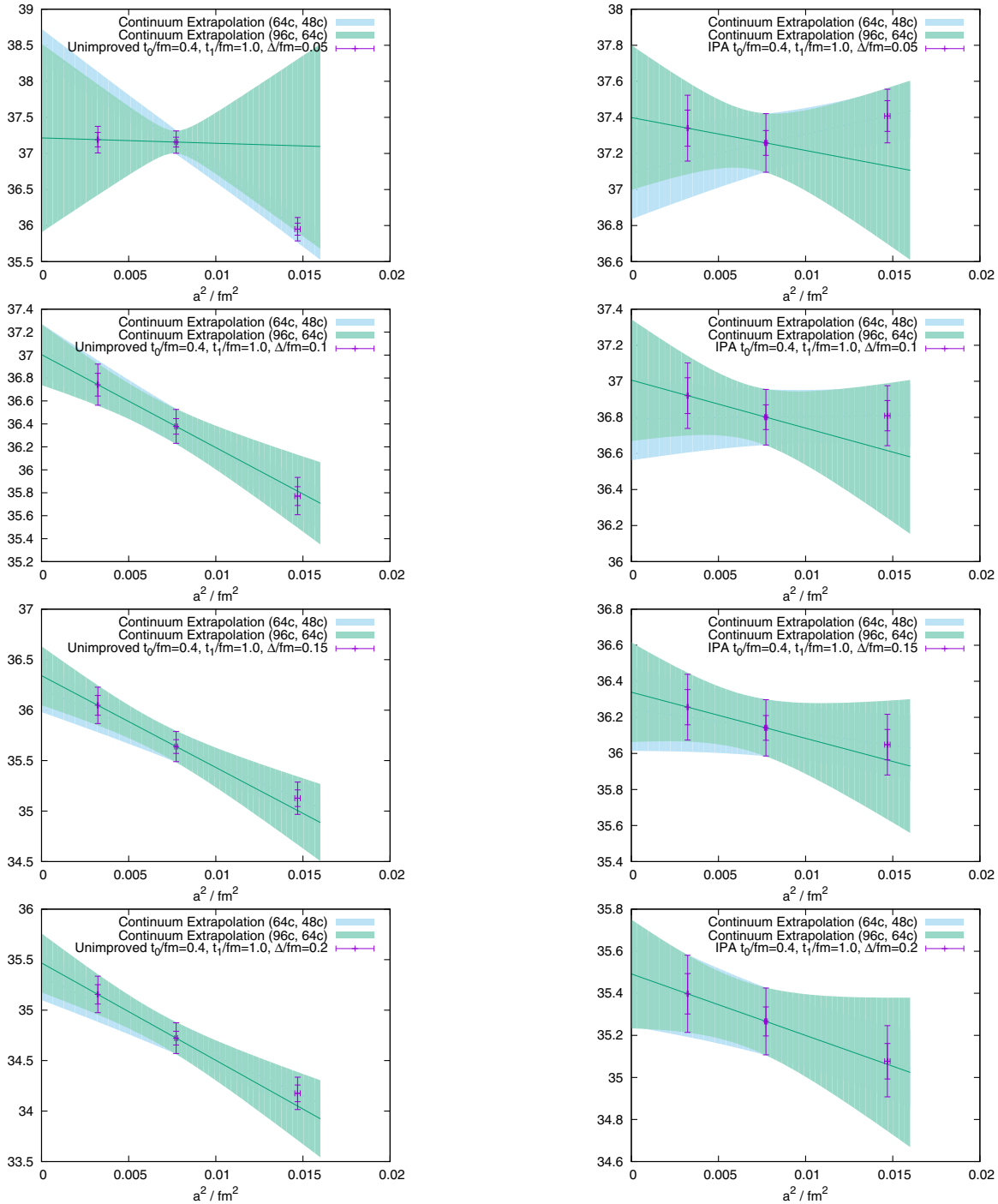


FIG. 8. Continuum extrapolations with $m_v/m_s = 1/3$ for various choices of window smearing Δ . All windows have $(t_0, t_1) = (0.4, 1.0)$ fm. The left and right columns are for the unimproved data and for the data with the parity improvement, respectively. The continuum-extrapolation errors are enhanced when Δ is too small, but the IPA softens this issue.

is only well motivated for quark masses close to the isospin-symmetric valence quark mass limit. Significant deviations from the unimproved data are seen in the $m_v/m_s = 1$ data, while the $m_v/m_s = 1/3$ data only exhibit tension at the $1 - 2\sigma$ level. Good agreement between the two procedures is observed for the $m_v/m_s = 1/12$ data.

C. Valence mass extrapolation

After the continuum extrapolation, the valence quark masses are extrapolated to the isospin-symmetric light-quark mass. The value obtained from this extrapolation gives the connected light-quark contribution to the HVP from Eq. (7). In addition to the intercept of this extrapolation, the slope also provides information about the strong- isospin-breaking

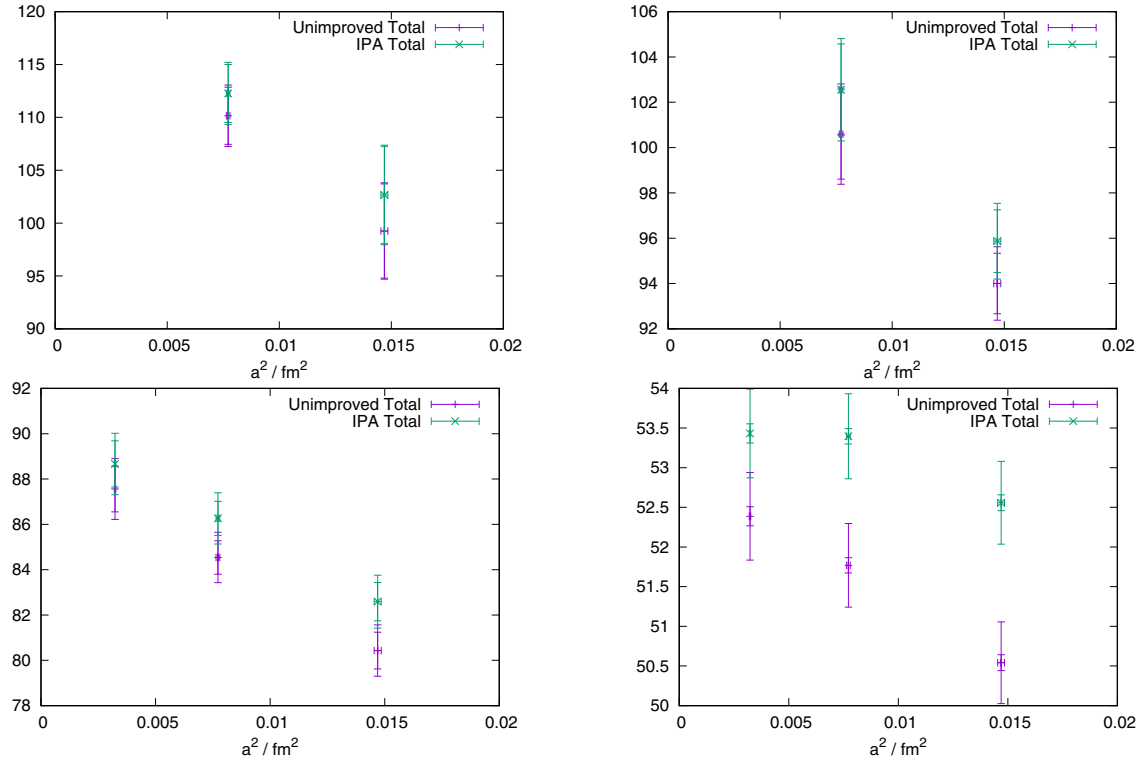


FIG. 9. Unimproved versus parity improved data as a function of lattice spacing. The upper-left, upper-right, lower-left, and lower-right plots have $m_v/m_s = 1/12, 1/6, 1/3$, and 1, respectively. The parity improved data with ρ parameters is not well motivated for the strange-quark masses and is not used for the final analysis.

given in Eq. (10). No extrapolation is needed to get to $m_v = m_s$ since this calculation is performed explicitly.

Figure 10 shows the extrapolation in valence quark mass for both the total contribution and for the window with $(t_0, t_1) = (0.4, 1.0)$ fm. Both statistical and systematic errors are included, and all data have been extrapolated to the continuum. In this figure, the IPA procedure is not performed and the \hat{p} prescription is used in all windows.

The mass dependence of the short-distance ρ resonance states is very linear over most of the range between the light and strange-quark masses, while the long-distance $\pi\pi$ states give a noticeable curvature. The fit parameters for the extrapolation in valence quark masses for each of the windows is given in Table IV.

Figure 11 shows the valence quark data extrapolated to the isospin-symmetric limit for a few choices of

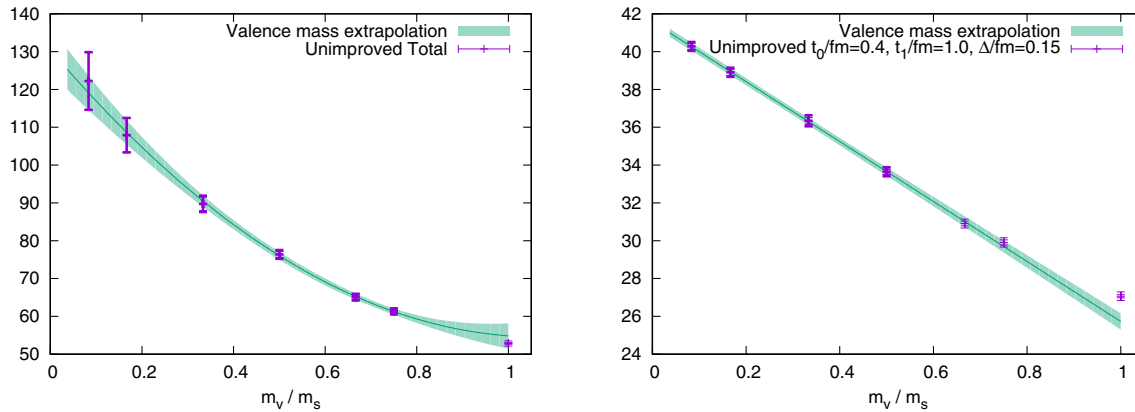


FIG. 10. Valence mass extrapolation of a_μ^v for the total time extent (left) and for the window with $(t_0, t_1) = (0.4, 1.0)$ fm (right). The points are the continuum-extrapolated data and the shaded region is the mass extrapolation. For the rather short-distance window, a linear extrapolation is sufficient, while a quadratic fit is needed for the total result including long distances. The fit parameters for each window are given in Table IV and the points included in the central fit are highlighted in the figure. The extrapolated band must be multiplied by a factor of 5 when comparing to the light-quark results in Table V; see Eq. (7).

TABLE IV. List of fit parameters for the valence mass extrapolation in each window. The fits are parametrized as degree d polynomials of m_v/m_s , including the n lightest masses. A fit is repeated with the k lightest masses to estimate the systematic error due to the valence extrapolation and is added as a systematic uncertainty. This uncertainty is included in the systematic error band in Figs. 10 and 11.

t_0/fm	t_1/fm	Δ/fm	d	n	k
Total			2	6	5
0.0	0.1	0.15	1	4	3
0.1	0.2	0.15	1	4	3
0.2	0.3	0.15	1	4	3
0.3	0.4	0.15	1	4	3
0.4	0.5	0.15	1	4	3
0.5	0.6	0.15	1	4	3
0.6	0.7	0.15	1	4	3
0.7	0.8	0.15	1	4	3
0.8	0.9	0.15	1	4	3
0.9	1.0	0.15	1	4	3
1.0	1.1	0.15	2	5	4
1.1	1.2	0.15	2	5	4
1.2	1.3	0.15	2	5	4
1.3	1.4	0.15	2	5	4
1.4	1.5	0.15	2	5	4
1.5	1.6	0.15	2	5	4
1.6	1.7	0.15	2	7	6
1.7	1.8	0.15	2	7	6
1.8	1.9	0.15	2	7	6
1.9	2.0	0.15	2	7	6
0.3	1.0	0.15	1	4	3
0.3	1.3	0.15	2	5	4
0.3	1.6	0.15	2	5	4
0.4	1.0	0.15	1	4	3
0.4	1.3	0.15	2	5	4
0.4	1.6	0.15	2	5	4
0.4	1.0	0.05	1	4	3
0.4	1.0	0.1	1	4	3
0.4	1.0	0.2	1	4	3

$t_1 - t_0 = 0.1$ fm windows. The first two windows with $t_0 = 0.4$ fm and $t_0 = 0.9$ fm are linear over a large mass range. The third window shows clear evidence of curvature in the valence quark mass, and therefore motivates the switch from a linear to a quadratic fit ansatz. The curvature continues to increase with increasing t_0 .

Table V shows the results for a series of time ranges and widths after extrapolation to the light-quark mass. These results are repeated in Tables X–XIII in Appendix with all systematic uncertainties shown in detail. For all windows, the p and \hat{p} prescriptions give results that are 1σ consistent. The parity improvement also gives consistent results with unimproved data for windows with $t_0 \geq 0.4$ fm. Short windows with t_0 and t_1 close to 0 fm are also subject to much larger discretization errors from the continuum extrapolation than wider window regions or those farther from 0 fm. For

instance, the window with $(t_0, t_1) = (0.0, 0.2)$ fm has a smaller relative systematic uncertainty than the window with $(t_0, t_1) = (0.0, 0.1)$ fm. The parity improvement is not well motivated for very short-distance windows and we give the results only for completeness.

D. Corrections for finite volume

The finite-volume correction (FVC) is a correction to the long-distance physics in the correlation function due to the finite spatial extent of the lattice. The lattice states in the long-distance region are mostly composed of two-pion scattering states with zero center-of-mass momentum, up to mixing with other states that share the same quantum numbers. The finite spatial extent imposes a lower limit on the size of a unit of momentum, $p = 2\pi/L$, which discretizes the spectrum of states that satisfy the periodic boundary conditions. The lowest-energy state in the spectrum of the connected isospin-1 channel is a two-pion state with both pions having one unit of momentum back-to-back. In infinite volume, where there is no minimum momentum, two-pion states would contribute all the way down to the two-pion threshold energy $s = 4M_\pi^2$, significantly changing the long-distance exponential tail of the correlation function. The FVC attempts to fix this mismatch of the finite and infinite volume.

The estimate of the FVC is obtained from the Lellouch-Lüscher-Gounaris-Sakurai procedure [61–64]. This is carried out by combining the pion form factor with estimates of the finite- and infinite-volume spectrum and matrix elements. In the infinite volume, the pion form factor is related to $R(s)$ via

$$R(s) = \frac{1}{4} \left(1 - \frac{4M_\pi^2}{s} \right)^{3/2} |F_\pi(s)|^2, \quad (28)$$

and $R(s)$ is inserted into Eq. (2) to obtain the $\pi\pi$ contribution to the correlation function $C(t)$. The pion form factor $F_\pi(s)$ used in $R(s)$ is obtained from the Gounaris-Sakurai (GS) parametrization [61]. The pion scattering phase shift for obtaining the finite-volume spectrum and matrix elements is computed with GS parametrization as well, which has the simple relation

$$F_\pi(s) = f(0)/f(s), \quad (29)$$

with

$$f(s) = (-i + \cot \delta_1(s)) \frac{k_\pi(s)^3}{\sqrt{s}}, \quad (30)$$

where

$$k_\pi(s) = \sqrt{\frac{1}{4}s - M_\pi^2} \quad (31)$$

is the pion momentum for the center of mass energy \sqrt{s} . The phase shift $\delta_1(s)$ is related to the finite-volume spectrum according to the relation [62]

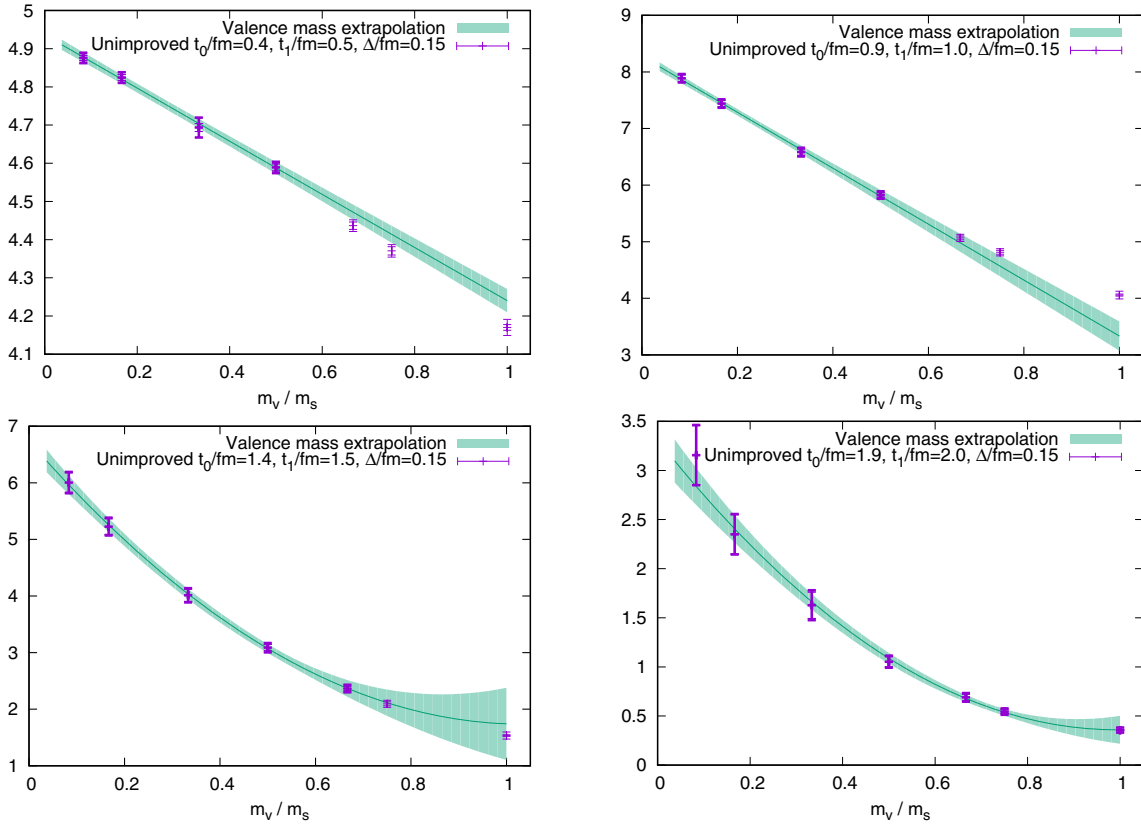


FIG. 11. Valence mass extrapolation for four different windows. The points are the continuum-extrapolated data and the shaded region is the mass extrapolation. For short-distance windows, a linear extrapolation is sufficient, while a quadratic fit is needed for long-distance windows. The fit parameters for each window are given in Table IV, and the points included in the central fit are bold.

$$\delta_1(s) + \phi(q) = n\pi, \quad n \in \mathbb{Z}, \quad (32)$$

where $q(s) = (L/2\pi)k_\pi(s)$ and $\phi(q)$ is determined from

$$\tan \phi(q) = -\frac{\pi^{3/2} q}{\mathcal{Z}_{00}(1; q)}, \quad (33)$$

with the analytic continuation of the zeta function

$$\mathcal{Z}_{00}(s; q) = \frac{1}{\sqrt{4\pi}} \sum_{\vec{n} \in \mathbb{Z}^3} \frac{1}{(|\vec{n}|^2 - q^2)^s}. \quad (34)$$

For a set of finite-volume states obtained by solving Eq. (32), the corresponding vector current amplitudes are obtained from [63,64]

$$\begin{aligned} & |\langle 0 | V_i | \pi\pi(\sqrt{s} = E_{\pi\pi}) \rangle|^2 \\ &= |F_\pi(E_{\pi\pi}^2)|^2 \frac{2k_\pi^4}{3\pi E_{\pi\pi}^2} \left[\frac{\partial}{\partial k_\pi} (\delta_1 + \phi) \right]^{-1}. \end{aligned} \quad (35)$$

The $C(t)$ obtained from both the infinite-volume parametrization of F_π and from the explicit reconstruction of a finite number of states N ,

$$C^{\text{FV}}(t) = \sum_n^N |\langle 0 | V_i | \pi\pi_n \rangle|^2 e^{-E_{\pi\pi_n} t}, \quad (36)$$

are both summed with the Bernecker-Meyer kernel w_t as in Eq. (1). The finite-volume correction for the connected diagram is then

$$\Delta a_\mu^{\text{FVC}} = \frac{10}{9} \sum_{t=0}^{\infty} w_t [C^{\text{IV}}(t) - C^{\text{FV}}(t)], \quad (37)$$

where C^{IV} denotes the infinite-volume correlation function. The factor 10/9 arises for the connected compared to the total contribution [50,65].

These numbers are listed in Table VI for the full result and windows. To estimate the finite-volume correction, $C^{\text{FV}}(t)$ is reconstructed with 12 states. The difference between the 11- and 12-state reconstructions is added as a systematic error. An additional 30% uncertainty on the correction is applied to cover other uncontrolled systematic effects associated with the finite-volume corrections.

The size of the contribution from each light and strange window and the size of the finite-volume correction for the light-quark mass for each of the $t_1 - t_0 = 0.1$ fm windows

TABLE V. Results for $a_\mu^{\text{ud,conn.,isospin}}$, labeled by “l”, and $a_\mu^{\text{s,conn.,isospin}}$, labeled by “s”, for the total contribution as well as different windows. We compare results obtained from the \hat{p} and p prescriptions as well as unimproved (U) and IPA (I) results. The IPA procedure is defined in Sec. II C. The value for the full time range is given in the first row, labeled “Total.” All windows with $t_0 \geq 0.4$ fm are consistent for all four choices of prescription and improvement. For windows with lower t_0 , discretization effects account for significant differences in the window sums. The IPA prescription, however, is not well motivated for small distances. We use the \hat{p} and unimproved prescriptions for our central values further discussed in the following. We notice that broader windows with $t_1 - t_0 = 0.2$ fm have smaller relative systematic uncertainties for small t_0 compared to the narrower windows.

t_0/fm	t_1/fm	Δ/fm	$l, \hat{p}\text{U}$	$l, \hat{p}\text{I}$	$l, p\text{U}$	$l, p\text{I}$	$s, \hat{p}\text{U}$	$s, p\text{U}$
Total			627(26)(08)	632(27)(07)	628(26)(07)	634(27)(07)	52.83(22)(65)	53.08(22)(82)
0.0	0.1	0.15	3.59(00)(59)	4.60(00)(31)	4.32(00)(20)	5.69(00)(24)	0.81(00)(12)	0.887(00)(40)
0.1	0.2	0.15	8.633(03)(73)	9.93(00)(52)	9.29(00)(46)	11.0(0.0)(1.3)	1.666(01)(12)	1.728(01)(86)
0.2	0.3	0.15	14.24(01)(82)	15.4(0.0)(1.3)	14.7(0.0)(1.2)	16.0(0.0)(1.8)	2.57(00)(16)	2.59(00)(24)
0.3	0.4	0.15	18.62(02)(35)	20.2(0.0)(1.1)	18.71(02)(27)	20.3(0.0)(1.3)	3.448(05)(65)	3.451(05)(49)
0.4	0.5	0.15	24.552(35)(60)	24.71(04)(24)	24.518(36)(59)	24.65(04)(21)	4.170(07)(20)	4.169(08)(24)
0.5	0.6	0.15	29.38(06)(29)	29.42(06)(26)	29.36(06)(31)	29.36(06)(31)	4.666(10)(59)	4.665(11)(64)
0.6	0.7	0.15	33.72(10)(36)	33.87(10)(26)	33.70(10)(39)	33.82(10)(29)	4.866(13)(74)	4.866(13)(79)
0.7	0.8	0.15	37.54(14)(14)	37.30(15)(19)	37.54(15)(14)	37.28(15)(20)	4.799(16)(39)	4.799(16)(39)
0.8	0.9	0.15	39.32(20)(20)	39.52(21)(18)	39.33(21)(20)	39.52(21)(18)	4.505(17)(44)	4.504(18)(44)
0.9	1.0	0.15	40.47(27)(29)	40.43(28)(28)	40.47(27)(30)	40.44(28)(28)	4.058(19)(65)	4.058(19)(65)
1.0	1.1	0.15	40.47(44)(39)	40.56(46)(37)	40.49(45)(39)	40.57(46)(37)	3.527(19)(76)	3.527(19)(76)
1.1	1.2	0.15	39.34(54)(39)	39.47(56)(43)	39.35(55)(39)	39.48(57)(44)	2.973(19)(75)	2.973(19)(75)
1.2	1.3	0.15	37.53(65)(49)	37.54(67)(48)	37.55(66)(49)	37.56(68)(48)	2.441(18)(77)	2.440(18)(77)
1.3	1.4	0.15	34.88(77)(49)	34.98(79)(51)	34.89(77)(49)	35.00(80)(52)	1.955(17)(67)	1.955(17)(67)
1.4	1.5	0.15	31.94(88)(52)	31.98(91)(53)	31.96(89)(52)	31.99(92)(53)	1.534(15)(60)	1.534(15)(60)
1.5	1.6	0.15	28.66(100)(52)	28.7(1.0)(0.5)	28.7(1.0)(0.5)	28.7(1.0)(0.5)	1.181(13)(52)	1.181(13)(52)
1.6	1.7	0.15	24.58(81)(61)	24.64(82)(62)	24.59(81)(61)	24.65(83)(62)	0.894(12)(44)	0.894(12)(44)
1.7	1.8	0.15	21.20(85)(60)	21.28(86)(62)	21.21(85)(60)	21.20(86)(55)	0.667(10)(37)	0.667(10)(37)
1.8	1.9	0.15	18.13(86)(59)	18.22(88)(63)	18.13(87)(60)	18.23(88)(63)	0.491(08)(30)	0.491(08)(30)
1.9	2.0	0.15	15.49(89)(66)	15.42(91)(50)	15.37(89)(46)	15.57(91)(70)	0.357(07)(24)	0.357(07)(25)
0.0	0.2	0.15	12.22(00)(52)	14.53(00)(21)	13.61(00)(26)	16.7(0.0)(1.5)	2.48(00)(11)	2.615(02)(47)
0.2	0.4	0.15	32.87(03)(48)	35.6(0.0)(2.4)	33.41(03)(94)	36.3(0.0)(3.0)	6.02(01)(10)	6.05(01)(19)
0.4	0.6	0.15	53.93(10)(28)	54.12(10)(13)	53.88(10)(33)	54.00(10)(17)	8.837(18)(74)	8.834(18)(85)
0.6	0.8	0.15	71.26(24)(37)	71.16(25)(44)	71.23(24)(40)	71.11(25)(49)	9.666(29)(91)	9.665(29)(97)
0.8	1.0	0.15	79.80(47)(42)	79.96(49)(44)	79.81(48)(42)	79.96(49)(44)	8.56(04)(10)	8.56(04)(10)
0.3	1.0	0.15	223.6(0.8)(1.1)	225.5(0.8)(1.2)	223.6(0.8)(1.1)	225.4(0.8)(1.2)	30.51(08)(25)	30.51(09)(26)
0.3	1.3	0.15	340.7(2.6)(1.9)	343.4(2.7)(2.7)	340.7(2.6)(1.9)	343.3(2.7)(2.7)	39.45(13)(35)	39.45(13)(35)
0.3	1.6	0.15	436.2(5.1)(3.1)	439.0(5.3)(4.2)	436.3(5.1)(3.2)	439.5(5.3)(4.0)	44.12(17)(49)	44.12(17)(49)
0.4	1.0	0.15	204.99(79)(85)	205.25(82)(77)	204.93(80)(90)	205.08(83)(83)	27.06(08)(21)	27.06(08)(22)
0.4	1.3	0.15	322.2(2.6)(1.8)	322.8(2.7)(1.9)	322.2(2.6)(1.8)	321.6(2.7)(2.1)	36.01(13)(36)	36.00(13)(35)
0.4	1.6	0.15	417.7(5.1)(3.2)	418.5(5.3)(3.4)	417.9(5.1)(3.2)	418.3(5.3)(3.3)	40.68(17)(51)	40.67(17)(50)
0.4	1.0	0.05	215.5(0.8)(6.2)	208.5(0.8)(1.5)	215.8(0.8)(6.4)	208.4(0.8)(1.6)	27.9(0.1)(1.1)	27.9(0.1)(1.1)
0.4	1.0	0.1	208.85(77)(74)	207.6(0.8)(1.1)	208.76(78)(70)	207.4(0.8)(1.3)	27.70(08)(21)	27.69(08)(20)
0.4	1.0	0.2	201.08(82)(85)	201.86(85)(77)	201.10(84)(86)	201.83(86)(76)	26.24(08)(21)	26.24(08)(21)

are shown in Fig. 12. The upper panel shows the window result from $t_0 = t - 0.05$ fm to $t_1 = t + 0.05$ fm with $\Delta = 0.15$ fm for both the isospin-symmetric connected light-quark as well as strange-quark contribution. The lower panel shows the size of the FVC to the light-quark mass contribution for each of the windows. These numbers are provided in Table VI. For the strange-quark contribution, we assume FVC to be negligible. We combine these FVC with the finite-volume isospin-symmetric light-quark connected windows to our final results for $a_\mu^{\text{ud,conn.,isospin}}$ and $a_\mu^{\text{s,conn.,isospin}}$ in Table VII.

Since at leading order in Δm the pion-mass splitting is a pure QED effect, it is expected that two-pion contributions to the total SIB contribution largely cancel. This is, however, not true for the connected and disconnected pieces (diagrams M and O of Fig. 2) separately. In particular, when connected and disconnected SIB corrections are compared between different lattice collaborations, performed at different volumes, this is important to take into account.

In order to address this issue, we use NLO PQChPT [50,65], which yields a correlator for the connected and disconnected diagrams of Fig. 1,

TABLE VI. Finite-volume corrections for each window. The numbers for the light-quark connected isospin-symmetric contribution are plotted in the bottom panel of Fig. 12.

t_0/fm	t_1/fm	Δ/fm	$\Delta a_\mu^{\text{ud,conn.,isospin}} 10^{10}$	$\Delta a_\mu^{\text{SIB,conn.}} 10^{10}$
Total			29.9(9.0)	3.8(1.1)
0.0	0.1	0.15	0.0068(21)	0.000103(32)
0.1	0.2	0.15	0.0162(50)	0.000320(100)
0.2	0.3	0.15	0.0299(92)	0.00085(26)
0.3	0.4	0.15	0.046(14)	0.00195(60)
0.4	0.5	0.15	0.065(20)	0.0039(12)
0.5	0.6	0.15	0.089(27)	0.0069(21)
0.6	0.7	0.15	0.123(38)	0.0112(34)
0.7	0.8	0.15	0.169(52)	0.0168(52)
0.8	0.9	0.15	0.229(70)	0.0238(73)
0.9	1.0	0.15	0.301(93)	0.0320(98)
1.0	1.1	0.15	0.38(12)	0.041(13)
1.1	1.2	0.15	0.47(15)	0.051(16)
1.2	1.3	0.15	0.57(17)	0.062(19)
1.3	1.4	0.15	0.66(20)	0.072(22)
1.4	1.5	0.15	0.76(23)	0.083(25)
1.5	1.6	0.15	0.85(26)	0.093(28)
1.6	1.7	0.15	0.93(28)	0.102(31)
1.7	1.8	0.15	1.00(30)	0.110(34)
1.8	1.9	0.15	1.05(32)	0.117(36)
1.9	2.0	0.15	1.10(33)	0.123(38)
0.0	0.2	0.15	0.0230(71)	0.00042(13)
0.2	0.4	0.15	0.076(23)	0.00280(87)
0.4	0.6	0.15	0.154(47)	0.0108(33)
0.6	0.8	0.15	0.293(90)	0.0279(86)
0.8	1.0	0.15	0.53(16)	0.056(17)
0.3	1.0	0.15	1.02(31)	0.096(30)
0.3	1.3	0.15	2.45(75)	0.251(77)
0.3	1.6	0.15	4.7(1.4)	0.50(15)
0.4	1.0	0.15	0.98(30)	0.094(29)
0.4	1.3	0.15	2.40(74)	0.249(76)
0.4	1.6	0.15	4.7(1.4)	0.50(15)
0.4	1.0	0.05	0.92(28)	0.088(27)
0.4	1.0	0.1	0.94(29)	0.091(28)
0.4	1.0	0.2	1.02(31)	0.099(31)

$$C^{\text{NLO,PQChPT,conn.}}(t) = \frac{10}{9} \frac{1}{3} \frac{1}{L^3} \sum_{\vec{p}} \frac{\vec{p}^2}{(E_p^{vl})^2} e^{-2E_p^{vl} t}, \quad (38)$$

$$C^{\text{NLO,PQChPT,disc.}}(t) = -\frac{1}{9} \frac{1}{3} \frac{1}{L^3} \sum_{\vec{p}} \frac{\vec{p}^2}{(E_p^{vv})^2} e^{-2E_p^{vv} t}, \quad (39)$$

with

$$E_p^{vl} = \sqrt{(m_\pi^{vl})^2 + \vec{p}^2}, \quad E_p^{vv} = \sqrt{(m_\pi^{vv})^2 + \vec{p}^2},$$

$$(m_\pi^{vl})^2 = B(m_l + m_v), \quad (m_\pi^{vv})^2 = 2Bm_v. \quad (40)$$

In these expressions, L^3 is the spatial volume. We then use Eqs. (11) and (12), to relate this correlator to diagram M and O, for which we can compute finite-volume corrections. We find

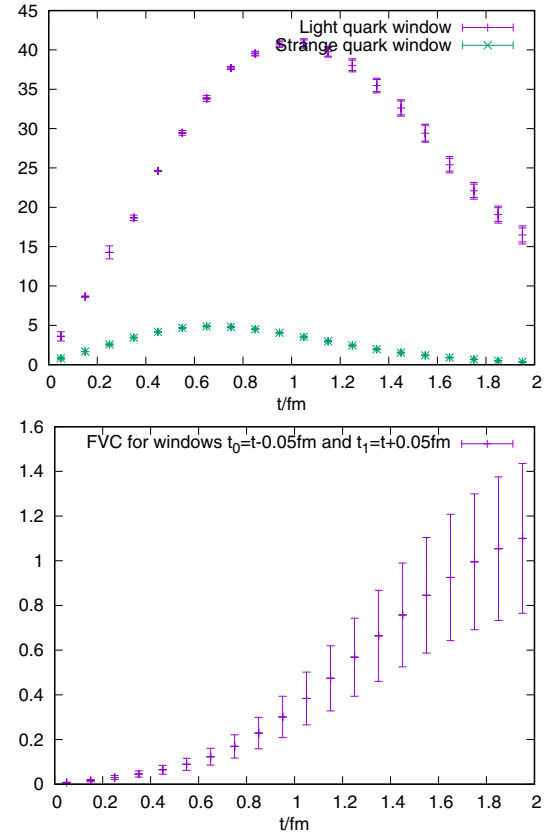


FIG. 12. The top panel shows the continuum, infinite-volume limit of the connected isospin-symmetric light and strange windows with $t_0 = t - 0.05$ fm and $t_1 = t + 0.05$ fm and $\Delta = 0.15$ fm. The bottom panel shows the FVC for light valence quark mass in the isospin-symmetric limit. The continuum limit of the very short-distance windows is difficult to control as described in Sec. II.

$$\frac{\partial}{\partial m_v} C^{\text{NLO,PQChPT,conn.}} = \frac{5}{9} \frac{\partial}{\partial m_v} c = -\frac{10}{9} M, \quad (41)$$

$$\frac{\partial}{\partial m_v} C^{\text{NLO,PQChPT,disc.}} = -\frac{1}{9} \frac{\partial}{\partial m_v} d = \frac{2}{9} O. \quad (42)$$

From Eq. (38), it then follows that

$$\begin{aligned} & \left. \frac{\partial}{\partial m_v} C^{\text{NLO,PQChPT,conn.}} \right|_{m_v=m_l} \\ &= -5 \left. \frac{\partial}{\partial m_v} C^{\text{NLO,PQChPT,disc.}} \right|_{m_v=m_l} \end{aligned} \quad (43)$$

and therefore that within NLO PQChPT,

$$M = O. \quad (44)$$

Since the connected plus disconnected SIB enters as $M - O$, indeed the total two-pion contributions cancel. In this work, we use the separate expressions for the connected and disconnected SIB FVC and quote the appropriate

TABLE VII. Final results, including finite-volume corrections, for connected isospin-symmetric light and strange-quark contributions.

t_0/fm	t_1/fm	Δ/fm	$a_\mu^{\text{ud,conn.,isospin}} 10^{10}$	$a_\mu^{\text{s,conn.,isospin}} 10^{10}$
Total			657(26)(12)	52.83(22)(65)
0.0	0.1	0.15	3.60(00)(59)	0.81(00)(12)
0.1	0.2	0.15	8.649(03)(73)	1.666(01)(12)
0.2	0.3	0.15	14.27(01)(82)	2.57(00)(16)
0.3	0.4	0.15	18.67(02)(35)	3.448(05)(65)
0.4	0.5	0.15	24.617(35)(63)	4.170(07)(20)
0.5	0.6	0.15	29.47(06)(29)	4.666(10)(59)
0.6	0.7	0.15	33.85(10)(37)	4.866(13)(74)
0.7	0.8	0.15	37.71(14)(15)	4.799(16)(39)
0.8	0.9	0.15	39.55(20)(21)	4.505(17)(44)
0.9	1.0	0.15	40.77(27)(31)	4.058(19)(65)
1.0	1.1	0.15	40.86(44)(41)	3.527(19)(76)
1.1	1.2	0.15	39.81(54)(42)	2.973(19)(75)
1.2	1.3	0.15	38.10(65)(51)	2.441(18)(77)
1.3	1.4	0.15	35.54(77)(53)	1.955(17)(67)
1.4	1.5	0.15	32.70(88)(56)	1.534(15)(60)
1.5	1.6	0.15	29.50(100)(58)	1.181(13)(52)
1.6	1.7	0.15	25.51(81)(66)	0.894(12)(44)
1.7	1.8	0.15	22.20(85)(66)	0.667(10)(37)
1.8	1.9	0.15	19.18(86)(67)	0.491(08)(30)
1.9	2.0	0.15	16.59(89)(75)	0.357(07)(24)
0.0	0.2	0.15	12.25(00)(52)	2.48(00)(11)
0.2	0.4	0.15	32.95(03)(48)	6.02(01)(10)
0.4	0.6	0.15	54.08(10)(29)	8.837(18)(74)
0.6	0.8	0.15	71.55(24)(38)	9.666(29)(91)
0.8	1.0	0.15	80.33(47)(44)	8.56(04)(10)
0.3	1.0	0.15	224.6(0.8)(1.1)	30.51(08)(25)
0.3	1.3	0.15	343.1(2.6)(2.0)	39.45(13)(35)
0.3	1.6	0.15	441.0(5.1)(3.4)	44.12(17)(49)
0.4	1.0	0.15	205.97(79)(90)	27.06(08)(21)
0.4	1.3	0.15	324.6(2.6)(1.9)	36.01(13)(36)
0.4	1.6	0.15	422.4(5.1)(3.5)	40.68(17)(51)
0.4	1.0	0.05	216.5(0.8)(6.2)	27.9(0.1)(1.1)
0.4	1.0	0.1	209.80(77)(79)	27.70(08)(21)
0.4	1.0	0.2	202.10(82)(91)	26.24(08)(21)

TABLE VIII. We combine new results obtained in this paper with results for the missing contributions from RBC/UKQCD [21] to our total result for a_μ^{HVPLO} .

Contribution	Result $\times 10^{10}$	From
Total	714(27)(13)	
ud, conn., isospin	657(26)(12)	Table VII
s, conn., isospin	52.83(22)(65)	Table VII
c, conn., isospin	14.3(0.0)(0.7)	Ref. [21]
uds, disc., isospin	-11.2(3.3)(2.3)	Ref. [21]
SIB, conn.	9.0(0.8)(1.2)	Table IX
SIB, disc.	-6.9(0.0)(3.5)	Eq. (45)
QED, conn.	5.9(5.7)(1.7)	Ref. [21]
QED, disc.	-6.9(2.1)(2.0)	Ref. [21]

infinite-volume result for $a_\mu^{\text{SIB,conn.}}$ in addition to the finite-volume result $a_\mu^{\text{SIB,conn.,fv}}$ for different windows in Table IX.

It is instructive to consider the infinite-volume NLO PQChPT results,

$$a_\mu^{\text{SIB,conn.,NLOPQ}_\chi\text{PT}} = -a_\mu^{\text{SIB,disc.,NLOPQ}_\chi\text{PT}} \quad (45)$$

$$= 6.9(3.5)10^{-10}, \quad (46)$$

where we add a 50% systematic error. In these expressions, we use $m_\pi = 135$ MeV since in this context we are interested in the evaluation of mass derivatives at the isospin-symmetric limit ($m_v = m_l$).

TABLE IX. We provide results for the connected SIB contribution both at finite volume ($a_\mu^{\text{SIB,conn.,fv}}$) and at infinite volume $a_\mu^{\text{SIB,conn.}}$. While the sum of the connected and disconnected SIB contribution have likely small finite-volume corrections, $a_\mu^{\text{SIB,conn.}}$ itself receives a significant correction. This is important for comparisons of this contribution between different lattice results.

t_0/fm	t_1/fm	Δ/fm	$a_\mu^{\text{SIB,conn.,fv}} 10^{10}$	$a_\mu^{\text{SIB,conn.}} 10^{10}$
Total			5.25(76)(29)	9.0(0.8)(1.2)
0.0	0.1	0.15	-0.002(00)(17)	-0.002(00)(17)
0.1	0.2	0.15	0.0015(01)(23)	0.0019(01)(23)
0.2	0.3	0.15	0.007(00)(23)	0.008(00)(23)
0.3	0.4	0.15	0.009(01)(11)	0.011(01)(11)
0.4	0.5	0.15	0.0266(10)(16)	0.0305(10)(22)
0.5	0.6	0.15	0.0462(16)(91)	0.0531(16)(93)
0.6	0.7	0.15	0.077(02)(11)	0.088(02)(12)
0.7	0.8	0.15	0.1159(35)(66)	0.1327(35)(90)
0.8	0.9	0.15	0.1502(46)(76)	0.174(05)(11)
0.9	1.0	0.15	0.189(06)(14)	0.221(06)(18)
1.0	1.1	0.15	0.255(20)(19)	0.296(20)(24)
1.1	1.2	0.15	0.296(24)(22)	0.348(24)(28)
1.2	1.3	0.15	0.331(27)(29)	0.393(27)(36)
1.3	1.4	0.15	0.348(31)(29)	0.420(31)(38)
1.4	1.5	0.15	0.356(34)(30)	0.439(34)(41)
1.5	1.6	0.15	0.351(37)(27)	0.443(37)(41)
1.6	1.7	0.15	0.297(18)(26)	0.399(18)(42)
1.7	1.8	0.15	0.270(18)(25)	0.381(18)(43)
1.8	1.9	0.15	0.243(18)(24)	0.361(18)(44)
1.9	2.0	0.15	0.219(18)(26)	0.342(18)(47)
0.0	0.2	0.15	-0.001(00)(14)	-0.000(00)(14)
0.2	0.4	0.15	0.016(01)(13)	0.019(01)(13)
0.4	0.6	0.15	0.0729(26)(83)	0.0836(26)(91)
0.6	0.8	0.15	0.193(06)(12)	0.221(06)(16)
0.8	1.0	0.15	0.339(10)(19)	0.395(10)(27)
0.3	1.0	0.15	0.615(19)(35)	0.711(19)(49)
0.3	1.3	0.15	1.47(12)(10)	1.72(12)(13)
0.3	1.6	0.15	2.53(21)(17)	3.03(21)(24)
0.4	1.0	0.15	0.606(18)(31)	0.700(18)(46)
0.4	1.3	0.15	1.47(12)(10)	1.72(12)(13)
0.4	1.6	0.15	2.53(21)(18)	3.03(21)(25)
0.4	1.0	0.05	0.63(02)(19)	0.72(02)(20)
0.4	1.0	0.1	0.603(18)(35)	0.693(18)(48)
0.4	1.0	0.2	0.615(19)(31)	0.715(19)(47)

V. DISCUSSION AND CONCLUSION

We summarize our results for the total contributions to a_μ^{HVPLO} in Table VIII and compare this result in Fig. 14 to results by other collaborations. In Fig. 13, we compare our results for $a_\mu^{\text{ud,conn.,isospin}}$, $a_\mu^{\text{SIB,conn.}}$, and the window

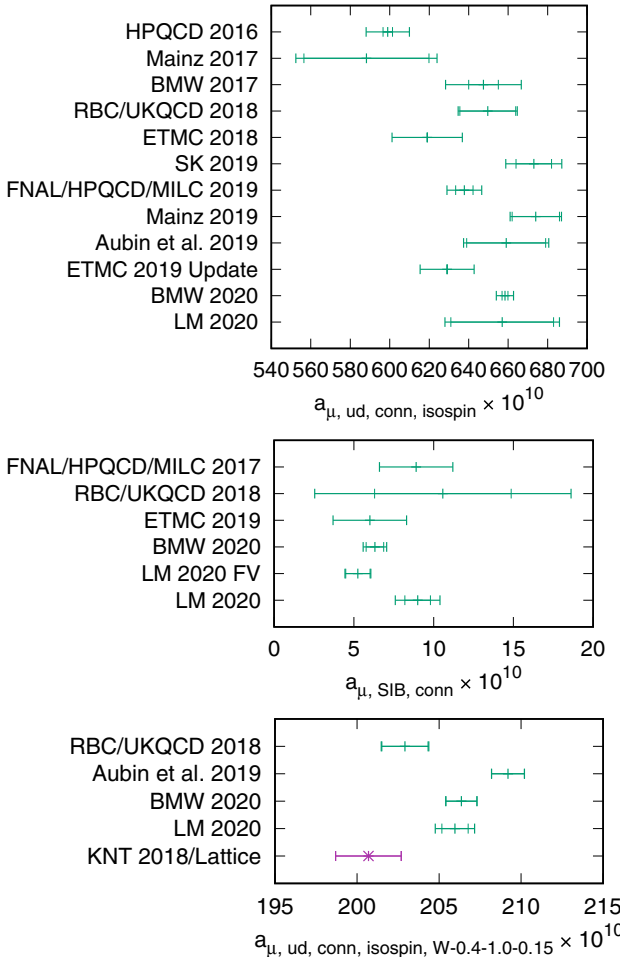


FIG. 13. Overview of results for $a_\mu^{\text{ud,conn.,isospin}}$, $a_\mu^{\text{SIB,conn.}}$, and the window $a_\mu^{\text{ud,conn.,isospin},W}$ with $t_0 = 0.4$ fm, $t_1 = 1.0$ fm, and $\Delta = 0.15$ fm. The referenced contributions are listed in the caption of Fig. 14 apart from ETMC 2019 [29] and FNAL/HPQCD/MILC 2017 [17]. The result of this work is labeled “LM 2020.” For $a_\mu^{\text{ud,conn.,isospin}}$, the precise BMW 2020 is higher in particular compared to values by ETMC 2019 Update as well as FNAL/HPQCD/MILC 2019. For $a_\mu^{\text{SIB,conn.}}$, we provide also a finite-volume result “LM 2020 FV” to compare to the other results obtained at similar volume. LM 2020 is the value corrected to infinite volume. For the window $a_\mu^{\text{ud,conn.,isospin},W}$, there is a clear tension between Aubin *et al.* [50,66] and the R ratio as well as RBC/UKQCD 2018. In this work, we perform a calculation on the same gauge configurations as Aubin *et al.* 2019 but with a different discretization of the vector current and find a substantially lower value. This difference may therefore originate from difficulties associated with the continuum limit. In Fig. 15, we provide an overview of a broader set of individual contributions to the HVP.

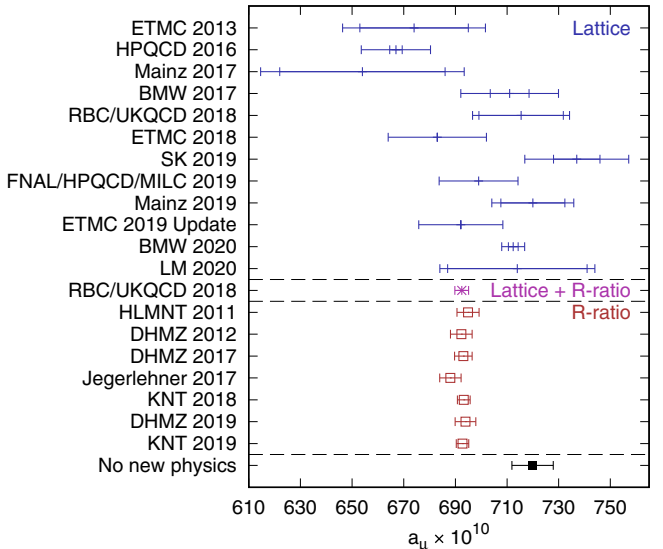


FIG. 14. Overview of total results for a_μ^{HVP} . The referenced contributions are ETMC 2013 [11], HPQCD 2016 [14], Mainz 2017 [19], BMW 2017 [20], RBC/UKQCD 2018 [21], ETMC 2018 [22], SK 2019 [25], FNAL/HPQCD/MILC 2019 [24], Mainz 2019 [26], ETMC 2019 Update [30], BMW 2020 [27], HLMNT 2011 [6], DHMZ 2012 [7], DHMZ 2017 [8], Jegerlehner 2017 [9], KNT 2018 [10], DHMZ 2019 [1], and KNT 2019 [2]. The result of this work is labeled “LM 2020.”

$a_\mu^{\text{ud,conn.,isospin},W}$ with $t_0 = 0.4$ fm, $t_1 = 1.0$ fm, and $\Delta = 0.15$ fm to other collaborations. We would like to stress in particular the difference between the window results from Aubin *et al.* and this work, which is especially noteworthy since they were performed on the same gauge configurations. Apart from the small valence mass extrapolation, which we suggest to be mild for the window, the main difference between this work and Aubin *et al.* is the choice of a site-local current compared to a conserved current. This suggests that properly estimating the uncertainties associated with the continuum limit may be challenging. We note that in this work, Aubin *et al.*, as well as the recent BMW result, results at similar inverse lattice spacings from $a^{-1} \approx 1.6$ GeV to $a^{-1} \approx 3.5$ GeV were used, all with staggered sea quark ensembles at physical pion mass.

We hope that the larger set of window results provided in this work can be useful to further scrutinize the emerging tensions within the lattice QCD community and within lattice QCD and the R ratio. We expect that in the near future other lattice collaborations will also provide results for the total a_μ^{HVPLO} with uncertainties close to 5×10^{-10} , which may shed further light on the emerging tensions. It will be particularly important that such results include different lattice discretizations.

ACKNOWLEDGMENTS

We thank our colleagues in the RBC and UKQCD Collaborations for interesting discussions. We thank the

MILC Collaboration for the ensembles used in this analysis. Inversions and contractions were performed with the MILC code version 7. This work was supported by resources provided by the Scientific Data and Computing Center (SDCC) at Brookhaven National Laboratory (BNL), a DOE Office of Science User Facility supported by the Office of Science of the U.S. Department of Energy. The SDCC is a major component of the Computational Science Initiative at BNL. We gratefully acknowledge computing resources provided through USQCD clusters at BNL and Jefferson Lab. C. L. and A. S. M. are supported in part by U.S. DOE Award No. DESC0012704(BNL) and by a DOE Office of Science Early Career Award.

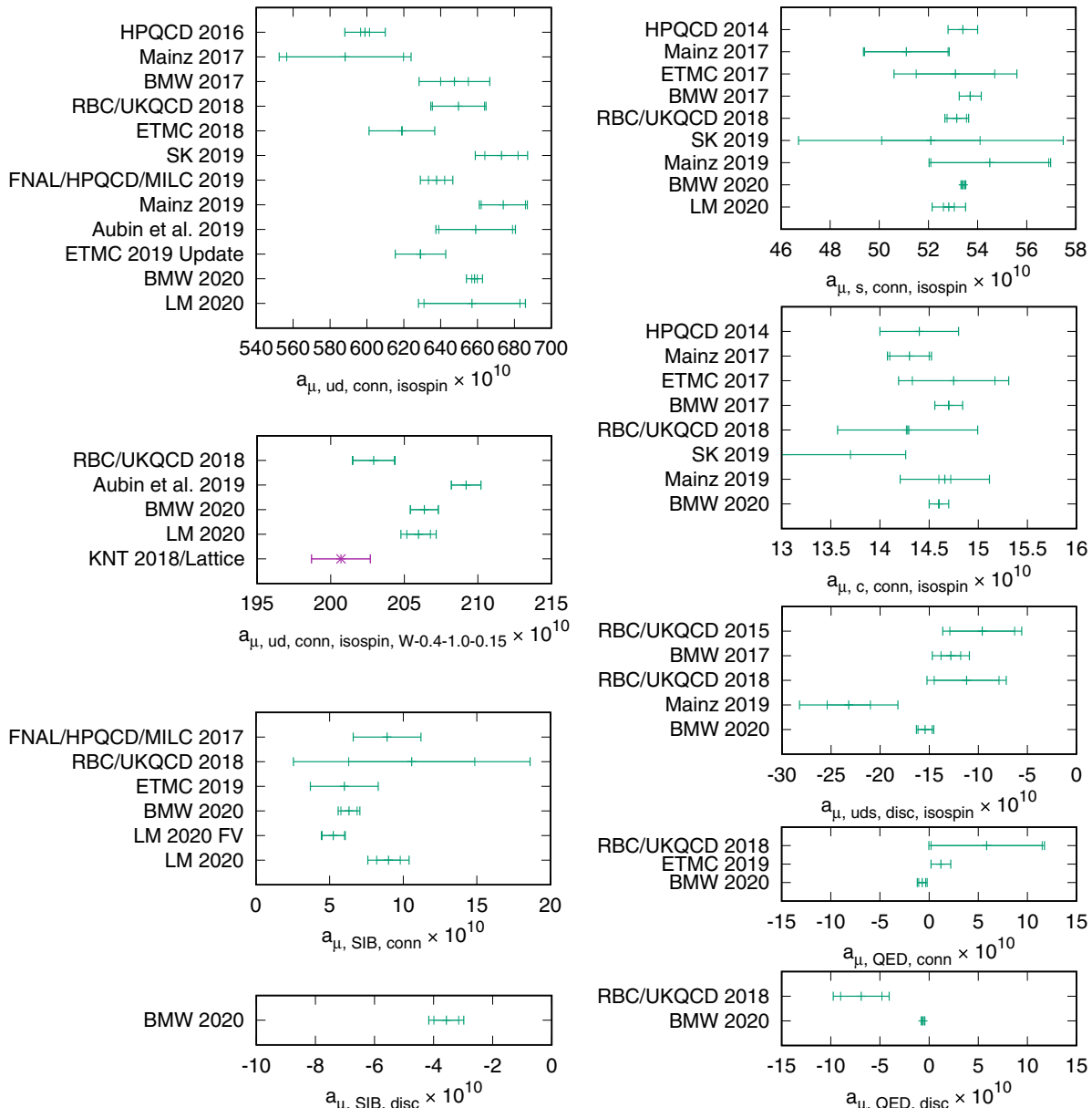


FIG. 15. Overview of individual contributions to a_μ^{HVP} . The result of this work is labeled LM 2020. The references are defined in the captions of Figs. 13 and 14.

APPENDIX: RESULTS

This section contains tables with a detailed breakdown of systematic errors from the window data that appear in Table V. Tables X and XI give the systematic error breakdown for the \hat{p} prescription, while Tables XII and XIII give the p prescription. Tables X and XII both contain unimproved data, while Tables XI and XIII both use the IPA procedure of Sec. II C. All of Tables X–XIII use the light-quark mass data. Tables XIV and XV give the unimproved data with the \hat{p} and p prescriptions for the strange-quark mass, respectively.

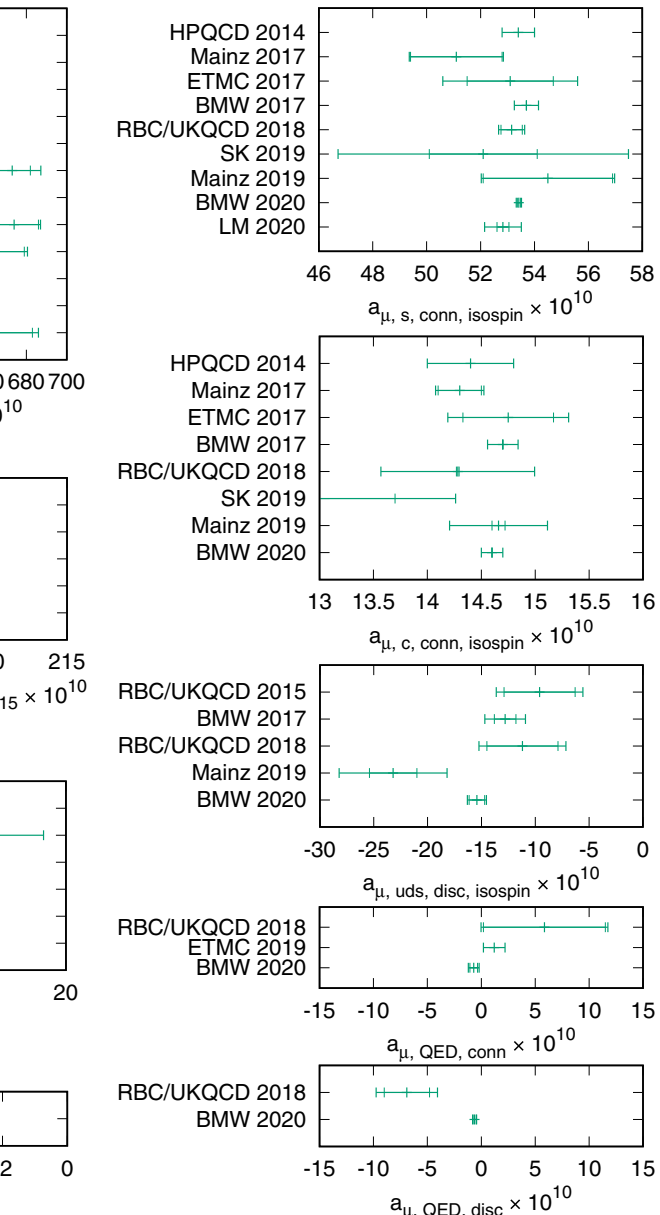


TABLE X. A detailed breakdown of the systematic uncertainties for the data in the column labeled $l, \hat{p}U$ in Table V. These are the unimproved data with the \hat{p} prescription applied. The subscripts on each uncertainty denote the different sources of uncertainty. In cases where each ensemble has a different uncertainty, a superscript of 48, 64, or 96 is included to indicate the 48c, 64c, or 96c ensemble, respectively. The subscript S denotes the statistical error. The subscript Z_V indicates the uncertainty on the vector current renormalization factors, which are given in Table I. The subscript C_3 indicates the continuum limit uncertainty on the $m_v/m_s = 1/3$ ensemble, which is used to inform the shift on the other valence quark masses. The uncertainty obtained from the continuum limit of the other valence quark masses is collected into the subscript C . We notice significant fluctuations of the short-distance window continuum error estimates since for the $t_0 = 0.1$ fm, $t_1 = 0.2$ fm window the 48c-64c and 64c-96c continuum extrapolations are in fortuitous agreement. This indicates limits of the reliability of the corresponding error estimate. The subscript $\frac{m_l}{m_s}$ denotes the uncertainty propagated from λ_0 , m_l denotes the uncertainty from the light sea-quark mistuning, and $\frac{m_v}{m_s}$ denotes the light quark mass extrapolation uncertainty. The subscript w_0/a denotes the scale setting uncertainty from the corresponding values in Table I, and the subscript w_0 from the value in the caption of Table I.

t_0/fm	t_1/fm	Δ/fm	$a_\mu^{\text{ud,conn.,isospin,W}} \times 10^{10}$
Total			$627(26)_S(00)_{Z_V^{48}}(00)_{Z_V^{64}}(02)_{Z_V^{96}}(03)_{C_3}(00)_C(03)_{m_l}(00)\frac{m_l}{m_s}(02)\frac{m_v}{m_s}(00)\frac{w_0}{a^{48}}(00)\frac{w_0}{a^{64}}(01)\frac{w_0}{a^{96}}(06)_{w_0}$
0.0	0.1	0.15	$3.59(00)_S(00)_{Z_V^{48}}(00)_{Z_V^{64}}(00)_{Z_V^{96}}(06)_{C_3}(52)_C(00)_{m_l}(00)\frac{m_l}{m_s}(26)\frac{m_v}{m_s}(00)\frac{w_0}{a^{48}}(00)\frac{w_0}{a^{64}}(01)\frac{w_0}{a^{96}}(01)_{w_0}$
0.1	0.2	0.15	$8.633(03)_S(04)_{Z_V^{48}}(13)_{Z_V^{64}}(02)_{Z_V^{96}}(06)_{C_3}(63)_C(01)_{m_l}(00)\frac{m_l}{m_s}(32)\frac{m_v}{m_s}(00)\frac{w_0}{a^{48}}(01)\frac{w_0}{a^{64}}(00)\frac{w_0}{a^{96}}(10)_{w_0}$
0.2	0.3	0.15	$14.24(01)_S(01)_{Z_V^{48}}(02)_{Z_V^{64}}(01)_{Z_V^{96}}(09)_{C_3}(73)_C(00)_{m_l}(00)\frac{m_l}{m_s}(36)\frac{m_v}{m_s}(00)\frac{w_0}{a^{48}}(00)\frac{w_0}{a^{64}}(00)\frac{w_0}{a^{96}}(02)_{w_0}$
0.3	0.4	0.15	$18.62(02)_S(01)_{Z_V^{48}}(03)_{Z_V^{64}}(01)_{Z_V^{96}}(03)_{C_3}(30)_C(00)_{m_l}(00)\frac{m_l}{m_s}(16)\frac{m_v}{m_s}(00)\frac{w_0}{a^{48}}(00)\frac{w_0}{a^{64}}(00)\frac{w_0}{a^{96}}(01)_{w_0}$
0.4	0.5	0.15	$24.552(35)_S(20)_{Z_V^{48}}(49)_{Z_V^{64}}(03)_{Z_V^{96}}(03)_{C_3}(19)_C(14)_{m_l}(00)\frac{m_l}{m_s}(10)\frac{m_v}{m_s}(01)\frac{w_0}{a^{48}}(01)\frac{w_0}{a^{64}}(00)\frac{w_0}{a^{96}}(07)_{w_0}$
0.5	0.6	0.15	$29.38(06)_S(02)_{Z_V^{48}}(05)_{Z_V^{64}}(01)_{Z_V^{96}}(03)_{C_3}(25)_C(02)_{m_l}(00)\frac{m_l}{m_s}(13)\frac{m_v}{m_s}(00)\frac{w_0}{a^{48}}(00)\frac{w_0}{a^{64}}(00)\frac{w_0}{a^{96}}(03)_{w_0}$
0.6	0.7	0.15	$33.72(10)_S(03)_{Z_V^{48}}(06)_{Z_V^{64}}(01)_{Z_V^{96}}(03)_{C_3}(32)_C(04)_{m_l}(00)\frac{m_l}{m_s}(15)\frac{m_v}{m_s}(01)\frac{w_0}{a^{48}}(01)\frac{w_0}{a^{64}}(00)\frac{w_0}{a^{96}}(02)_{w_0}$
0.7	0.8	0.15	$37.54(14)_S(03)_{Z_V^{48}}(07)_{Z_V^{64}}(01)_{Z_V^{96}}(00)_{C_3}(03)_C(06)_{m_l}(00)\frac{m_l}{m_s}(04)\frac{m_v}{m_s}(01)\frac{w_0}{a^{48}}(01)\frac{w_0}{a^{64}}(00)\frac{w_0}{a^{96}}(08)_{w_0}$
0.8	0.9	0.15	$39.32(20)_S(03)_{Z_V^{48}}(07)_{Z_V^{64}}(01)_{Z_V^{96}}(02)_{C_3}(09)_C(08)_{m_l}(00)\frac{m_l}{m_s}(02)\frac{m_v}{m_s}(01)\frac{w_0}{a^{48}}(02)\frac{w_0}{a^{64}}(00)\frac{w_0}{a^{96}}(14)_{w_0}$
0.9	1.0	0.15	$40.47(27)_S(03)_{Z_V^{48}}(07)_{Z_V^{64}}(02)_{Z_V^{96}}(01)_{C_3}(12)_C(10)_{m_l}(00)\frac{m_l}{m_s}(16)\frac{m_v}{m_s}(02)\frac{w_0}{a^{48}}(02)\frac{w_0}{a^{64}}(01)\frac{w_0}{a^{96}}(17)_{w_0}$
1.0	1.1	0.15	$40.47(44)_S(04)_{Z_V^{48}}(10)_{Z_V^{64}}(03)_{Z_V^{96}}(01)_{C_3}(20)_C(14)_{m_l}(00)\frac{m_l}{m_s}(11)\frac{m_v}{m_s}(03)\frac{w_0}{a^{48}}(05)\frac{w_0}{a^{64}}(02)\frac{w_0}{a^{96}}(25)_{w_0}$
1.1	1.2	0.15	$39.34(54)_S(04)_{Z_V^{48}}(09)_{Z_V^{64}}(02)_{Z_V^{96}}(00)_{C_3}(17)_C(16)_{m_l}(01)\frac{m_l}{m_s}(14)\frac{m_v}{m_s}(04)\frac{w_0}{a^{48}}(06)\frac{w_0}{a^{64}}(01)\frac{w_0}{a^{96}}(26)_{w_0}$
1.2	1.3	0.15	$37.53(65)_S(03)_{Z_V^{48}}(09)_{Z_V^{64}}(01)_{Z_V^{96}}(00)_{C_3}(19)_C(18)_{m_l}(01)\frac{m_l}{m_s}(23)\frac{m_v}{m_s}(04)\frac{w_0}{a^{48}}(06)\frac{w_0}{a^{64}}(01)\frac{w_0}{a^{96}}(32)_{w_0}$
1.3	1.4	0.15	$34.88(77)_S(03)_{Z_V^{48}}(07)_{Z_V^{64}}(01)_{Z_V^{96}}(00)_{C_3}(12)_C(19)_{m_l}(01)\frac{m_l}{m_s}(23)\frac{m_v}{m_s}(04)\frac{w_0}{a^{48}}(06)\frac{w_0}{a^{64}}(01)\frac{w_0}{a^{96}}(35)_{w_0}$
1.4	1.5	0.15	$31.94(88)_S(02)_{Z_V^{48}}(06)_{Z_V^{64}}(00)_{Z_V^{96}}(00)_{C_3}(14)_C(19)_{m_l}(01)\frac{m_l}{m_s}(26)\frac{m_v}{m_s}(04)\frac{w_0}{a^{48}}(06)\frac{w_0}{a^{64}}(00)\frac{w_0}{a^{96}}(37)_{w_0}$
1.5	1.6	0.15	$28.66(100)_S(02)_{Z_V^{48}}(05)_{Z_V^{64}}(00)_{Z_V^{96}}(00)_{C_3}(13)_C(19)_{m_l}(01)\frac{m_l}{m_s}(23)\frac{m_v}{m_s}(04)\frac{w_0}{a^{48}}(06)\frac{w_0}{a^{64}}(00)\frac{w_0}{a^{96}}(40)_{w_0}$
1.6	1.7	0.15	$24.58(81)_S(01)_{Z_V^{48}}(02)_{Z_V^{64}}(03)_{Z_V^{96}}(12)_{C_3}(00)_C(16)_{m_l}(01)\frac{m_l}{m_s}(42)\frac{m_v}{m_s}(02)\frac{w_0}{a^{48}}(02)\frac{w_0}{a^{64}}(05)\frac{w_0}{a^{96}}(39)_{w_0}$
1.7	1.8	0.15	$21.20(85)_S(01)_{Z_V^{48}}(02)_{Z_V^{64}}(03)_{Z_V^{96}}(10)_{C_3}(01)_C(15)_{m_l}(00)\frac{m_l}{m_s}(43)\frac{m_v}{m_s}(02)\frac{w_0}{a^{48}}(02)\frac{w_0}{a^{64}}(05)\frac{w_0}{a^{96}}(37)_{w_0}$
1.8	1.9	0.15	$18.13(86)_S(01)_{Z_V^{48}}(02)_{Z_V^{64}}(02)_{Z_V^{96}}(04)_{C_3}(00)_C(13)_{m_l}(00)\frac{m_l}{m_s}(47)\frac{m_v}{m_s}(02)\frac{w_0}{a^{48}}(02)\frac{w_0}{a^{64}}(04)\frac{w_0}{a^{96}}(33)_{w_0}$
1.9	2.0	0.15	$15.49(89)_S(01)_{Z_V^{48}}(01)_{Z_V^{64}}(02)_{Z_V^{96}}(06)_{C_3}(03)_C(12)_{m_l}(00)\frac{m_l}{m_s}(58)\frac{m_v}{m_s}(02)\frac{w_0}{a^{48}}(02)\frac{w_0}{a^{64}}(04)\frac{w_0}{a^{96}}(30)_{w_0}$
0.0	0.2	0.15	$12.22(00)_S(00)_{Z_V^{48}}(02)_{Z_V^{64}}(00)_{Z_V^{96}}(06)_{C_3}(46)_C(00)_{m_l}(00)\frac{m_l}{m_s}(23)\frac{m_v}{m_s}(00)\frac{w_0}{a^{48}}(00)\frac{w_0}{a^{64}}(00)\frac{w_0}{a^{96}}(02)_{w_0}$
0.2	0.4	0.15	$32.87(03)_S(02)_{Z_V^{48}}(06)_{Z_V^{64}}(01)_{Z_V^{96}}(05)_{C_3}(43)_C(01)_{m_l}(00)\frac{m_l}{m_s}(20)\frac{m_v}{m_s}(00)\frac{w_0}{a^{48}}(00)\frac{w_0}{a^{64}}(01)_{w_0}$
0.4	0.6	0.15	$53.93(10)_S(04)_{Z_V^{48}}(10)_{Z_V^{64}}(02)_{Z_V^{96}}(02)_{C_3}(23)_C(04)_{m_l}(00)\frac{m_l}{m_s}(11)\frac{m_v}{m_s}(00)\frac{w_0}{a^{48}}(00)\frac{w_0}{a^{64}}(00)\frac{w_0}{a^{96}}(02)_{w_0}$
0.6	0.8	0.15	$71.26(24)_S(06)_{Z_V^{48}}(14)_{Z_V^{64}}(02)_{Z_V^{96}}(03)_{C_3}(29)_C(10)_{m_l}(00)\frac{m_l}{m_s}(10)\frac{m_v}{m_s}(01)\frac{w_0}{a^{48}}(02)\frac{w_0}{a^{64}}(00)\frac{w_0}{a^{96}}(10)_{w_0}$
0.8	1.0	0.15	$79.80(47)_S(06)_{Z_V^{48}}(15)_{Z_V^{64}}(03)_{Z_V^{96}}(02)_{C_3}(04)_C(18)_{m_l}(01)\frac{m_l}{m_s}(14)\frac{m_v}{m_s}(03)\frac{w_0}{a^{48}}(04)\frac{w_0}{a^{64}}(01)\frac{w_0}{a^{96}}(30)_{w_0}$
0.3	1.0	0.15	$223.61(81)_S(18)_{Z_V^{48}}(42)_{Z_V^{64}}(06)_{Z_V^{96}}(08)_{C_3}(79)_C(33)_{m_l}(01)\frac{m_l}{m_s}(23)\frac{m_v}{m_s}(05)\frac{w_0}{a^{48}}(06)\frac{w_0}{a^{64}}(01)\frac{w_0}{a^{96}}(41)_{w_0}$
0.3	1.3	0.15	$340.7(2.6)_S(0.3)_{Z_V^{48}}(0.9)_{Z_V^{64}}(0.2)_{Z_V^{96}}(0.2)_{C_3}(0.5)_C(0.8)_{m_l}(0.0)\frac{m_l}{m_s}(0.4)\frac{m_v}{m_s}(0.2)\frac{w_0}{a^{48}}(0.3)\frac{w_0}{a^{64}}(0.1)\frac{w_0}{a^{96}}(1.2)_{w_0}$
0.3	1.6	0.15	$436.2(5.1)_S(0.4)_{Z_V^{48}}(1.0)_{Z_V^{64}}(0.2)_{Z_V^{96}}(0.1)_{C_3}(0.0)_C(1.4)_{m_l}(0.0)\frac{m_l}{m_s}(1.0)\frac{m_v}{m_s}(0.3)\frac{w_0}{a^{48}}(0.4)\frac{w_0}{a^{64}}(0.1)\frac{w_0}{a^{96}}(2.3)_{w_0}$
0.4	1.0	0.15	$204.99(79)_S(16)_{Z_V^{48}}(39)_{Z_V^{64}}(05)_{Z_V^{96}}(05)_{C_3}(48)_C(33)_{m_l}(01)\frac{m_l}{m_s}(07)\frac{m_v}{m_s}(05)\frac{w_0}{a^{48}}(06)\frac{w_0}{a^{64}}(01)\frac{w_0}{a^{96}}(42)_{w_0}$
0.4	1.3	0.15	$322.2(2.6)_S(0.3)_{Z_V^{48}}(0.8)_{Z_V^{64}}(0.2)_{Z_V^{96}}(0.1)_{C_3}(0.1)_C(0.8)_{m_l}(0.0)\frac{m_l}{m_s}(0.5)\frac{m_v}{m_s}(0.2)\frac{w_0}{a^{48}}(0.3)\frac{w_0}{a^{64}}(0.1)\frac{w_0}{a^{96}}(1.2)_{w_0}$
0.4	1.6	0.15	$417.7(5.1)_S(0.4)_{Z_V^{48}}(1.0)_{Z_V^{64}}(0.2)_{Z_V^{96}}(0.1)_{C_3}(0.4)_C(1.4)_{m_l}(0.0)\frac{m_l}{m_s}(1.2)\frac{m_v}{m_s}(0.3)\frac{w_0}{a^{48}}(0.4)\frac{w_0}{a^{64}}(0.1)\frac{w_0}{a^{96}}(2.3)_{w_0}$
0.4	1.0	0.05	$215.5(0.8)_S(0.2)_{Z_V^{48}}(0.4)_{Z_V^{64}}(0.1)_{Z_V^{96}}(0.6)_{C_3}(5.4)_C(0.3)_{m_l}(0.0)\frac{m_l}{m_s}(2.9)\frac{m_v}{m_s}(0.1)\frac{w_0}{a^{48}}(0.1)\frac{w_0}{a^{64}}(0.0)\frac{w_0}{a^{96}}(0.5)_{w_0}$
0.4	1.0	0.1	$208.85(77)_S(17)_{Z_V^{48}}(40)_{Z_V^{64}}(05)_{Z_V^{96}}(02)_{C_3}(23)_C(33)_{m_l}(01)\frac{m_l}{m_s}(25)\frac{m_v}{m_s}(05)\frac{w_0}{a^{48}}(06)\frac{w_0}{a^{64}}(01)\frac{w_0}{a^{96}}(36)_{w_0}$
0.4	1.0	0.2	$201.08(82)_S(16)_{Z_V^{48}}(38)_{Z_V^{64}}(06)_{Z_V^{96}}(06)_{C_3}(46)_C(33)_{m_l}(01)\frac{m_l}{m_s}(03)\frac{m_v}{m_s}(05)\frac{w_0}{a^{48}}(07)\frac{w_0}{a^{64}}(01)\frac{w_0}{a^{96}}(46)_{w_0}$

TABLE XI. Same as Table X, but with the parity improvement.

t_0/fm	t_1/fm	Δ/fm	$a_\mu^{\text{ud,conn,isospin,W}} \times 10^{10}$
Total			$632(27)_S(00)Z_V^{48}(00)Z_V^{64}(02)Z_V^{96}(00)C_3(00)C(03)m_l(00)\frac{m_l}{m_s}(01)\frac{m_s}{m_l}(00)\frac{w_0}{a^{48}}(00)\frac{w_0}{a^{64}}(01)\frac{w_0}{a^{96}}(06)w_0$
0.0	0.1	0.15	$4.60(00)_S(00)Z_V^{48}(01)Z_V^{64}(00)Z_V^{96}(03)C_3(28)C(00)m_l(00)\frac{m_l}{m_s}(14)\frac{m_p}{a^{48}}(00)\frac{w_0}{a^{64}}(00)\frac{w_0}{a^{96}}(01)w_0$
0.1	0.2	0.15	$9.93(00)_S(01)Z_V^{48}(01)Z_V^{64}(00)Z_V^{96}(06)C_3(46)C(00)m_l(00)\frac{m_l}{m_s}(23)\frac{m_p}{a^{48}}(00)\frac{w_0}{a^{64}}(00)\frac{w_0}{a^{96}}(00)w_0$
0.2	0.3	0.15	$15.4(0.0)_S(0.0)Z_V^{48}(0.0)Z_V^{64}(0.0)Z_V^{96}(0.1)C_3(1.1)C(0.0)m_l(0.0)\frac{m_l}{m_s}(0.6)\frac{m_p}{a^{48}}(0.0)\frac{w_0}{a^{64}}(0.0)\frac{w_0}{a^{96}}(0.0)w_0$
0.3	0.4	0.15	$20.2(0.0)_S(0.0)Z_V^{48}(0.0)Z_V^{64}(0.0)Z_V^{96}(0.1)C_3(1.0)C(0.0)m_l(0.0)\frac{m_l}{m_s}(0.5)\frac{m_p}{a^{48}}(0.0)\frac{w_0}{a^{64}}(0.0)\frac{w_0}{a^{96}}(0.0)w_0$
0.4	0.5	0.15	$24.71(04)_S(02)Z_V^{48}(05)Z_V^{64}(01)Z_V^{96}(02)C_3(21)C(01)m_l(00)\frac{m_l}{m_s}(09)\frac{m_p}{a^{48}}(00)\frac{w_0}{a^{64}}(00)\frac{w_0}{a^{96}}(01)w_0$
0.5	0.6	0.15	$29.42(06)_S(02)Z_V^{48}(06)Z_V^{64}(01)Z_V^{96}(02)C_3(22)C(03)m_l(00)\frac{m_l}{m_s}(11)\frac{m_p}{a^{48}}(00)\frac{w_0}{a^{64}}(00)\frac{w_0}{a^{96}}(01)w_0$
0.6	0.7	0.15	$33.87(10)_S(03)Z_V^{48}(06)Z_V^{64}(01)Z_V^{96}(02)C_3(22)C(04)m_l(00)\frac{m_l}{m_s}(10)\frac{m_p}{a^{48}}(00)\frac{w_0}{a^{64}}(01)\frac{w_0}{a^{96}}(00)\frac{w_0}{a^{96}}(04)w_0$
0.7	0.8	0.15	$37.30(15)_S(03)Z_V^{48}(07)Z_V^{64}(01)Z_V^{96}(01)C_3(13)C(06)m_l(00)\frac{m_l}{m_s}(04)\frac{m_p}{a^{48}}(01)\frac{w_0}{a^{64}}(01)\frac{w_0}{a^{96}}(00)\frac{w_0}{a^{96}}(08)w_0$
0.8	0.9	0.15	$39.52(21)_S(03)Z_V^{48}(07)Z_V^{64}(01)Z_V^{96}(01)C_3(01)C(08)m_l(00)\frac{m_l}{m_s}(04)\frac{m_p}{a^{48}}(02)\frac{w_0}{a^{64}}(00)\frac{w_0}{a^{96}}(13)w_0$
0.9	1.0	0.15	$40.43(28)_S(03)Z_V^{48}(07)Z_V^{64}(02)Z_V^{96}(00)C_3(08)C(10)m_l(00)\frac{m_l}{m_s}(14)\frac{m_p}{a^{48}}(02)\frac{w_0}{a^{64}}(02)\frac{w_0}{a^{96}}(01)\frac{w_0}{a^{96}}(18)w_0$
1.0	1.1	0.15	$40.56(46)_S(04)Z_V^{48}(10)Z_V^{64}(03)Z_V^{96}(01)C_3(19)C(14)m_l(00)\frac{m_l}{m_s}(12)\frac{m_p}{a^{48}}(03)\frac{w_0}{a^{64}}(05)\frac{w_0}{a^{96}}(01)\frac{w_0}{a^{96}}(23)w_0$
1.1	1.2	0.15	$39.47(56)_S(04)Z_V^{48}(10)Z_V^{64}(02)Z_V^{96}(01)C_3(20)C(16)m_l(01)\frac{m_l}{m_s}(17)\frac{m_p}{a^{48}}(04)\frac{w_0}{a^{64}}(06)\frac{w_0}{a^{96}}(01)\frac{w_0}{a^{96}}(27)w_0$
1.2	1.3	0.15	$37.54(67)_S(03)Z_V^{48}(09)Z_V^{64}(01)Z_V^{96}(00)C_3(18)C(18)m_l(01)\frac{m_l}{m_s}(22)\frac{m_p}{a^{48}}(04)\frac{w_0}{a^{64}}(06)\frac{w_0}{a^{96}}(01)\frac{w_0}{a^{96}}(32)w_0$
1.3	1.4	0.15	$34.98(79)_S(03)Z_V^{48}(07)Z_V^{64}(01)Z_V^{96}(00)C_3(15)C(19)m_l(01)\frac{m_l}{m_s}(26)\frac{m_p}{a^{48}}(04)\frac{w_0}{a^{64}}(06)\frac{w_0}{a^{96}}(01)\frac{w_0}{a^{96}}(35)w_0$
1.4	1.5	0.15	$31.98(91)_S(02)Z_V^{48}(06)Z_V^{64}(00)Z_V^{96}(00)C_3(14)C(19)m_l(01)\frac{m_l}{m_s}(27)\frac{m_p}{a^{48}}(04)\frac{w_0}{a^{64}}(06)\frac{w_0}{a^{96}}(00)\frac{w_0}{a^{96}}(38)w_0$
1.5	1.6	0.15	$28.7(1.0)_S(0.0)Z_V^{48}(0.1)Z_V^{64}(0.0)Z_V^{96}(0.0)C_3(0.1)C(0.2)m_l(0.0)\frac{m_l}{m_s}(0.2)\frac{m_p}{a^{48}}(0.0)\frac{w_0}{a^{64}}(0.1)\frac{w_0}{a^{96}}(0.0)\frac{w_0}{a^{96}}(0.4)w_0$
1.6	1.7	0.15	$24.64(82)_S(01)Z_V^{48}(02)Z_V^{64}(03)Z_V^{96}(13)C_3(00)C(16)m_l(01)\frac{m_l}{m_s}(43)\frac{m_p}{a^{48}}(02)\frac{w_0}{a^{64}}(05)\frac{w_0}{a^{96}}(39)w_0$
1.7	1.8	0.15	$21.28(86)_S(01)Z_V^{48}(02)Z_V^{64}(03)Z_V^{96}(10)C_3(01)C(15)m_l(00)\frac{m_l}{m_s}(46)\frac{m_p}{a^{48}}(02)\frac{w_0}{a^{64}}(05)\frac{w_0}{a^{96}}(37)w_0$
1.8	1.9	0.15	$18.22(88)_S(01)Z_V^{48}(01)Z_V^{64}(03)Z_V^{96}(04)C_3(00)C(13)m_l(00)\frac{m_l}{m_s}(51)\frac{m_p}{a^{48}}(02)\frac{w_0}{a^{64}}(02)\frac{w_0}{a^{96}}(04)\frac{w_0}{a^{96}}(34)w_0$
1.9	2.0	0.15	$15.42(91)_S(01)Z_V^{48}(01)Z_V^{64}(02)Z_V^{96}(08)C_3(03)C(12)m_l(00)\frac{m_l}{m_s}(37)\frac{m_p}{a^{48}}(02)\frac{w_0}{a^{64}}(04)\frac{w_0}{a^{96}}(31)w_0$
0.0	0.2	0.15	$14.53(00)_S(01)Z_V^{48}(02)Z_V^{64}(01)Z_V^{96}(02)C_3(19)C(00)m_l(00)\frac{m_l}{m_s}(09)\frac{m_p}{a^{48}}(00)\frac{w_0}{a^{64}}(00)\frac{w_0}{a^{96}}(01)w_0$
0.2	0.4	0.15	$35.6(0.0)_S(0.0)Z_V^{48}(0.1)Z_V^{64}(0.0)Z_V^{96}(0.3)C_3(2.2)C(0.0)m_l(0.0)\frac{m_l}{m_s}(1.1)\frac{m_p}{a^{48}}(0.0)\frac{w_0}{a^{64}}(0.0)\frac{w_0}{a^{96}}(0.0)w_0$
0.4	0.6	0.15	$54.12(10)_S(05)Z_V^{48}(11)Z_V^{64}(01)Z_V^{96}(00)C_3(01)C(04)m_l(00)\frac{m_l}{m_s}(02)\frac{m_p}{a^{48}}(00)\frac{w_0}{a^{64}}(00)\frac{w_0}{a^{96}}(03)w_0$
0.6	0.8	0.15	$71.16(25)_S(06)Z_V^{48}(14)Z_V^{64}(02)Z_V^{96}(03)C_3(36)C(10)m_l(00)\frac{m_l}{m_s}(14)\frac{m_p}{a^{48}}(01)\frac{w_0}{a^{64}}(02)\frac{w_0}{a^{96}}(00)\frac{w_0}{a^{96}}(11)w_0$
0.8	1.0	0.15	$79.96(49)_S(06)Z_V^{48}(14)Z_V^{64}(03)Z_V^{96}(01)C_3(07)C(18)m_l(01)\frac{m_l}{m_s}(18)\frac{m_p}{a^{48}}(03)\frac{w_0}{a^{64}}(04)\frac{w_0}{a^{96}}(01)\frac{w_0}{a^{96}}(31)w_0$
0.3	1.0	0.15	$225.47(83)_S(18)Z_V^{48}(42)Z_V^{64}(07)Z_V^{96}(07)C_3(74)C(34)m_l(01)\frac{m_l}{m_s}(49)\frac{m_p}{a^{48}}(05)\frac{w_0}{a^{64}}(06)\frac{w_0}{a^{96}}(02)\frac{w_0}{a^{96}}(47)w_0$
0.3	1.3	0.15	$343.4(2.7)_S(0.4)Z_V^{48}(0.9)Z_V^{64}(0.3)Z_V^{96}(0.2)C_3(1.6)C(0.8)m_l(0.0)\frac{m_l}{m_s}(1.1)\frac{m_p}{a^{48}}(0.2)\frac{w_0}{a^{64}}(0.3)\frac{w_0}{a^{96}}(0.1)\frac{w_0}{a^{96}}(1.3)w_0$
0.3	1.6	0.15	$439.0(5.3)_S(0.4)Z_V^{48}(1.1)Z_V^{64}(0.3)Z_V^{96}(0.2)C_3(2.0)C(1.4)m_l(0.0)\frac{m_l}{m_s}(2.0)\frac{m_p}{a^{48}}(0.3)\frac{w_0}{a^{64}}(0.5)\frac{w_0}{a^{96}}(0.1)\frac{w_0}{a^{96}}(2.4)w_0$
0.4	1.0	0.15	$205.25(82)_S(17)Z_V^{48}(39)Z_V^{64}(06)Z_V^{96}(04)C_3(29)C(33)m_l(01)\frac{m_l}{m_s}(05)\frac{m_p}{a^{48}}(06)\frac{w_0}{a^{64}}(01)\frac{w_0}{a^{96}}(45)w_0$
0.4	1.3	0.15	$322.8(2.7)_S(0.3)Z_V^{48}(0.8)Z_V^{64}(0.2)Z_V^{96}(0.1)C_3(0.2)C(0.8)m_l(0.0)\frac{m_l}{m_s}(0.6)\frac{m_p}{a^{48}}(0.2)\frac{w_0}{a^{64}}(0.3)\frac{w_0}{a^{96}}(0.1)\frac{w_0}{a^{96}}(1.3)w_0$
0.4	1.6	0.15	$418.5(5.3)_S(0.4)Z_V^{48}(1.0)Z_V^{64}(0.2)Z_V^{96}(0.0)C_3(0.7)C(1.4)m_l(0.0)\frac{m_l}{m_s}(1.4)\frac{m_p}{a^{48}}(0.3)\frac{w_0}{a^{64}}(0.5)\frac{w_0}{a^{96}}(0.1)\frac{w_0}{a^{96}}(2.4)w_0$
0.4	1.0	0.05	$208.5(0.8)_S(0.2)Z_V^{48}(0.4)Z_V^{64}(0.1)Z_V^{96}(0.1)C_3(1.1)C(0.3)m_l(0.0)\frac{m_l}{m_s}(0.5)\frac{m_p}{a^{48}}(0.0)\frac{w_0}{a^{64}}(0.1)\frac{w_0}{a^{96}}(0.0)\frac{w_0}{a^{96}}(0.7)w_0$
0.4	1.0	0.1	$207.60(79)_S(17)Z_V^{48}(40)Z_V^{64}(06)Z_V^{96}(09)C_3(84)C(32)m_l(01)\frac{m_l}{m_s}(29)\frac{m_p}{a^{48}}(05)\frac{w_0}{a^{64}}(06)\frac{w_0}{a^{96}}(01)\frac{w_0}{a^{96}}(43)w_0$
0.4	1.0	0.2	$201.86(85)_S(16)Z_V^{48}(38)Z_V^{64}(07)Z_V^{96}(01)C_3(08)C(33)m_l(01)\frac{m_l}{m_s}(23)\frac{m_p}{a^{48}}(05)\frac{w_0}{a^{64}}(07)\frac{w_0}{a^{96}}(02)\frac{w_0}{a^{96}}(48)w_0$

TABLE XII. Same as Table X, but with the p prescription.

t_0/fm	t_1/fm	Δ/fm	$a_\mu^{\text{ud,conn.,isospin,W}} \times 10^{10}$
Total			$628(26)_S(00)Z_V^{48}(00)Z_V^{64}(02)Z_V^{96}(02)_{C_3}(00)_C(03)_{m_l}(00)\frac{m_l}{m_s}(02)\frac{m_s}{m_l}(00)\frac{w_0}{a^{48}}(00)\frac{w_0}{a^{64}}(01)\frac{w_0}{a^{96}}(06)w_0$
0.0	0.1	0.15	$4.32(00)_S(00)Z_V^{48}(01)Z_V^{64}(00)Z_V^{96}(02)_{C_3}(18)_C(00)_{m_l}(00)\frac{m_l}{m_s}(09)\frac{m_p}{m_s}(00)\frac{w_0}{a^{48}}(00)\frac{w_0}{a^{64}}(01)\frac{w_0}{a^{96}}(01)w_0$
0.1	0.2	0.15	$9.29(00)_S(01)Z_V^{48}(02)Z_V^{64}(00)Z_V^{96}(05)_{C_3}(40)_C(00)_{m_l}(00)\frac{m_l}{m_s}(20)\frac{m_p}{m_s}(00)\frac{w_0}{a^{48}}(00)\frac{w_0}{a^{64}}(00)\frac{w_0}{a^{96}}(00)w_0$
0.2	0.3	0.15	$14.7(0.0)_S(0.0)Z_V^{48}(0.0)Z_V^{64}(0.0)Z_V^{96}(0.1)_{C_3}(1.1)_C(0.0)_{m_l}(0.0)\frac{m_l}{m_s}(0.5)\frac{m_p}{m_s}(0.0)\frac{w_0}{a^{48}}(0.0)\frac{w_0}{a^{64}}(0.0)\frac{w_0}{a^{96}}(0.0)w_0$
0.3	0.4	0.15	$18.71(02)_S(02)Z_V^{48}(04)Z_V^{64}(01)Z_V^{96}(03)_{C_3}(23)_C(00)_{m_l}(00)\frac{m_l}{m_s}(13)\frac{m_p}{m_s}(00)\frac{w_0}{a^{48}}(00)\frac{w_0}{a^{64}}(00)\frac{w_0}{a^{96}}(01)w_0$
0.4	0.5	0.15	$24.518(36)_S(22)Z_V^{48}(50)Z_V^{64}(04)Z_V^{96}(02)_{C_3}(13)_C(14)_{m_l}(00)\frac{m_l}{m_s}(03)\frac{m_p}{m_s}(01)\frac{w_0}{a^{48}}(00)\frac{w_0}{a^{64}}(00)\frac{w_0}{a^{96}}(08)w_0$
0.5	0.6	0.15	$29.36(06)_S(02)Z_V^{48}(06)Z_V^{64}(01)Z_V^{96}(03)_{C_3}(27)_C(02)_{m_l}(00)\frac{m_l}{m_s}(14)\frac{m_p}{m_s}(00)\frac{w_0}{a^{48}}(00)\frac{w_0}{a^{64}}(00)\frac{w_0}{a^{96}}(03)w_0$
0.6	0.7	0.15	$33.70(10)_S(03)Z_V^{48}(06)Z_V^{64}(01)Z_V^{96}(04)_{C_3}(34)_C(04)_{m_l}(00)\frac{m_l}{m_s}(17)\frac{m_p}{m_s}(01)\frac{w_0}{a^{48}}(01)\frac{w_0}{a^{64}}(00)\frac{w_0}{a^{96}}(02)w_0$
0.7	0.8	0.15	$37.54(15)_S(03)Z_V^{48}(07)Z_V^{64}(01)Z_V^{96}(00)_{C_3}(03)_C(06)_{m_l}(00)\frac{m_l}{m_s}(04)\frac{m_p}{m_s}(01)\frac{w_0}{a^{48}}(01)\frac{w_0}{a^{64}}(00)\frac{w_0}{a^{96}}(08)w_0$
0.8	0.9	0.15	$39.33(21)_S(03)Z_V^{48}(08)Z_V^{64}(01)Z_V^{96}(02)_{C_3}(09)_C(08)_{m_l}(00)\frac{m_l}{m_s}(02)\frac{m_p}{m_s}(01)\frac{w_0}{a^{48}}(02)\frac{w_0}{a^{64}}(00)\frac{w_0}{a^{96}}(14)w_0$
0.9	1.0	0.15	$40.47(27)_S(03)Z_V^{48}(07)Z_V^{64}(02)Z_V^{96}(01)_{C_3}(12)_C(10)_{m_l}(00)\frac{m_l}{m_s}(17)\frac{m_p}{m_s}(02)\frac{w_0}{a^{48}}(02)\frac{w_0}{a^{64}}(01)\frac{w_0}{a^{96}}(16)w_0$
1.0	1.1	0.15	$40.49(45)_S(04)Z_V^{48}(10)Z_V^{64}(03)Z_V^{96}(01)_{C_3}(21)_C(14)_{m_l}(00)\frac{m_l}{m_s}(11)\frac{m_p}{m_s}(03)\frac{w_0}{a^{48}}(05)\frac{w_0}{a^{64}}(02)\frac{w_0}{a^{96}}(25)w_0$
1.1	1.2	0.15	$39.35(55)_S(04)Z_V^{48}(09)Z_V^{64}(02)Z_V^{96}(00)_{C_3}(17)_C(16)_{m_l}(01)\frac{m_l}{m_s}(14)\frac{m_p}{m_s}(04)\frac{w_0}{a^{48}}(06)\frac{w_0}{a^{64}}(01)\frac{w_0}{a^{96}}(26)w_0$
1.2	1.3	0.15	$37.55(66)_S(03)Z_V^{48}(09)Z_V^{64}(01)Z_V^{96}(00)_{C_3}(20)_C(18)_{m_l}(01)\frac{m_l}{m_s}(23)\frac{m_p}{m_s}(04)\frac{w_0}{a^{48}}(06)\frac{w_0}{a^{64}}(01)\frac{w_0}{a^{96}}(32)w_0$
1.3	1.4	0.15	$34.89(77)_S(03)Z_V^{48}(07)Z_V^{64}(01)Z_V^{96}(00)_{C_3}(13)_C(19)_{m_l}(01)\frac{m_l}{m_s}(24)\frac{m_p}{m_s}(04)\frac{w_0}{a^{48}}(06)\frac{w_0}{a^{64}}(01)\frac{w_0}{a^{96}}(35)w_0$
1.4	1.5	0.15	$31.96(89)_S(02)Z_V^{48}(06)Z_V^{64}(00)Z_V^{96}(00)_{C_3}(14)_C(19)_{m_l}(01)\frac{m_l}{m_s}(26)\frac{m_p}{m_s}(04)\frac{w_0}{a^{48}}(06)\frac{w_0}{a^{64}}(00)\frac{w_0}{a^{96}}(37)w_0$
1.5	1.6	0.15	$28.7(1.0)_S(0.0)Z_V^{48}(0.1)Z_V^{64}(0.0)Z_V^{96}(0.0)_{C_3}(0.1)_C(0.2)_{m_l}(0.0)\frac{m_l}{m_s}(0.2)\frac{m_p}{m_s}(0.0)\frac{w_0}{a^{48}}(0.1)\frac{w_0}{a^{64}}(0.0)\frac{w_0}{a^{96}}(0.4)w_0$
1.6	1.7	0.15	$24.59(81)_S(01)Z_V^{48}(02)Z_V^{64}(03)Z_V^{96}(12)_{C_3}(00)_C(16)_{m_l}(01)\frac{m_l}{m_s}(42)\frac{m_p}{m_s}(02)\frac{w_0}{a^{48}}(02)\frac{w_0}{a^{64}}(05)\frac{w_0}{a^{96}}(39)w_0$
1.7	1.8	0.15	$21.21(85)_S(01)Z_V^{48}(02)Z_V^{64}(03)Z_V^{96}(11)_{C_3}(01)_C(15)_{m_l}(00)\frac{m_l}{m_s}(43)\frac{m_p}{m_s}(02)\frac{w_0}{a^{48}}(02)\frac{w_0}{a^{64}}(05)\frac{w_0}{a^{96}}(37)w_0$
1.8	1.9	0.15	$18.13(87)_S(01)Z_V^{48}(02)Z_V^{64}(02)Z_V^{96}(05)_{C_3}(00)_C(13)_{m_l}(00)\frac{m_l}{m_s}(47)\frac{m_p}{m_s}(02)\frac{w_0}{a^{48}}(02)\frac{w_0}{a^{64}}(04)\frac{w_0}{a^{96}}(33)w_0$
1.9	2.0	0.15	$15.37(89)_S(01)Z_V^{48}(01)Z_V^{64}(02)Z_V^{96}(06)_{C_3}(03)_C(11)_{m_l}(00)\frac{m_l}{m_s}(32)\frac{m_p}{m_s}(02)\frac{w_0}{a^{48}}(02)\frac{w_0}{a^{64}}(04)\frac{w_0}{a^{96}}(30)w_0$
0.0	0.2	0.15	$13.61(00)_S(01)Z_V^{48}(02)Z_V^{64}(00)Z_V^{96}(03)_{C_3}(23)_C(00)_{m_l}(00)\frac{m_l}{m_s}(12)\frac{m_p}{m_s}(00)\frac{w_0}{a^{48}}(00)\frac{w_0}{a^{64}}(00)\frac{w_0}{a^{96}}(01)w_0$
0.2	0.4	0.15	$33.41(03)_S(03)Z_V^{48}(06)Z_V^{64}(01)Z_V^{96}(10)_{C_3}(84)_C(01)_{m_l}(00)\frac{m_l}{m_s}(40)\frac{m_p}{m_s}(00)\frac{w_0}{a^{48}}(00)\frac{w_0}{a^{64}}(00)\frac{w_0}{a^{96}}(02)w_0$
0.4	0.6	0.15	$53.88(10)_S(05)Z_V^{48}(10)Z_V^{64}(02)Z_V^{96}(03)_{C_3}(28)_C(04)_{m_l}(00)\frac{m_l}{m_s}(14)\frac{m_p}{m_s}(00)\frac{w_0}{a^{48}}(00)\frac{w_0}{a^{64}}(00)\frac{w_0}{a^{96}}(02)w_0$
0.6	0.8	0.15	$71.23(24)_S(06)Z_V^{48}(14)Z_V^{64}(02)Z_V^{96}(03)_{C_3}(32)_C(10)_{m_l}(00)\frac{m_l}{m_s}(11)\frac{m_p}{m_s}(01)\frac{w_0}{a^{48}}(02)\frac{w_0}{a^{64}}(00)\frac{w_0}{a^{96}}(10)w_0$
0.8	1.0	0.15	$79.81(48)_S(06)Z_V^{48}(15)Z_V^{64}(03)Z_V^{96}(01)_{C_3}(04)_C(18)_{m_l}(01)\frac{m_l}{m_s}(14)\frac{m_p}{m_s}(03)\frac{w_0}{a^{48}}(04)\frac{w_0}{a^{64}}(01)\frac{w_0}{a^{96}}(30)w_0$
0.3	1.0	0.15	$223.63(82)_S(19)Z_V^{48}(43)Z_V^{64}(06)Z_V^{96}(08)_{C_3}(80)_C(33)_{m_l}(01)\frac{m_l}{m_s}(23)\frac{m_p}{m_s}(05)\frac{w_0}{a^{48}}(06)\frac{w_0}{a^{64}}(01)\frac{w_0}{a^{96}}(41)w_0$
0.3	1.3	0.15	$340.7(2.6)_S(0.4)Z_V^{48}(0.9)Z_V^{64}(0.2)Z_V^{96}(0.2)_{C_3}(0.5)_C(0.8)_{m_l}(0.0)\frac{m_l}{m_s}(0.4)\frac{m_p}{m_s}(0.2)\frac{w_0}{a^{48}}(0.3)\frac{w_0}{a^{64}}(0.1)\frac{w_0}{a^{96}}(1.2)w_0$
0.3	1.6	0.15	$436.3(5.1)_S(0.4)Z_V^{48}(1.1)Z_V^{64}(0.2)Z_V^{96}(0.1)_{C_3}(0.0)_C(1.4)_{m_l}(0.0)\frac{m_l}{m_s}(1.0)\frac{m_p}{m_s}(0.3)\frac{w_0}{a^{48}}(0.4)\frac{w_0}{a^{64}}(0.1)\frac{w_0}{a^{96}}(2.3)w_0$
0.4	1.0	0.15	$204.93(80)_S(17)Z_V^{48}(39)Z_V^{64}(06)Z_V^{96}(06)_{C_3}(56)_C(33)_{m_l}(01)\frac{m_l}{m_s}(11)\frac{m_p}{m_s}(05)\frac{w_0}{a^{48}}(06)\frac{w_0}{a^{64}}(01)\frac{w_0}{a^{96}}(42)w_0$
0.4	1.3	0.15	$322.2(2.6)_S(0.3)Z_V^{48}(0.8)Z_V^{64}(0.2)Z_V^{96}(0.1)_{C_3}(0.2)_C(0.8)_{m_l}(0.0)\frac{m_l}{m_s}(0.5)\frac{m_p}{m_s}(0.2)\frac{w_0}{a^{48}}(0.3)\frac{w_0}{a^{64}}(0.1)\frac{w_0}{a^{96}}(1.2)w_0$
0.4	1.6	0.15	$417.9(5.1)_S(0.4)Z_V^{48}(1.0)Z_V^{64}(0.2)Z_V^{96}(0.1)_{C_3}(0.3)_C(1.4)_{m_l}(0.0)\frac{m_l}{m_s}(1.0)\frac{m_p}{m_s}(0.3)\frac{w_0}{a^{48}}(0.5)\frac{w_0}{a^{64}}(0.1)\frac{w_0}{a^{96}}(2.3)w_0$
0.4	1.0	0.05	$215.8(0.8)_S(0.2)Z_V^{48}(0.4)Z_V^{64}(0.1)Z_V^{96}(0.6)_{C_3}(5.6)_C(0.3)_{m_l}(0.0)\frac{m_l}{m_s}(3.0)\frac{m_p}{m_s}(0.1)\frac{w_0}{a^{48}}(0.1)\frac{w_0}{a^{64}}(0.0)\frac{w_0}{a^{96}}(0.4)w_0$
0.4	1.0	0.1	$208.76(78)_S(17)Z_V^{48}(40)Z_V^{64}(05)Z_V^{96}(01)_{C_3}(13)_{m_l}(01)\frac{m_l}{m_s}(21)\frac{m_p}{m_s}(05)\frac{w_0}{a^{48}}(06)\frac{w_0}{a^{64}}(01)\frac{w_0}{a^{96}}(36)w_0$
0.4	1.0	0.2	$201.10(84)_S(17)Z_V^{48}(38)Z_V^{64}(06)Z_V^{96}(06)_{C_3}(48)_C(33)_{m_l}(01)\frac{m_l}{m_s}(03)\frac{m_p}{m_s}(05)\frac{w_0}{a^{48}}(07)\frac{w_0}{a^{64}}(01)\frac{w_0}{a^{96}}(46)w_0$

TABLE XIII. Same as Table XII, but with the parity improvement.

t_0/fm	t_1/fm	Δ/fm	$a_\mu^{\text{ud,conn.,isospin,W}} \times 10^{10}$
Total			$634(27)_S(00)Z_V^{48}(00)Z_V^{64}(01)Z_V^{96}(02)C_3(01)C(03)m_l(00)\frac{m_l}{m_s}(01)\frac{m_s}{m_l}(00)\frac{w_0}{a^{48}}(00)\frac{w_0}{a^{64}}(01)\frac{w_0}{a^{96}}(06)w_0$
0.0	0.1	0.15	$5.69(00)_S(00)Z_V^{48}(01)Z_V^{64}(00)Z_V^{96}(03)C_3(21)C(00)m_l(00)\frac{m_l}{m_s}(11)\frac{m_p}{m_s}(00)\frac{w_0}{a^{48}}(00)\frac{w_0}{a^{64}}(00)\frac{w_0}{a^{96}}(00)w_0$
0.1	0.2	0.15	$11.0(0.0)_S(0.0)Z_V^{48}(0.0)Z_V^{64}(0.0)Z_V^{96}(0.1)C_3(1.1)C(0.0)m_l(0.0)\frac{m_l}{m_s}(0.6)\frac{m_p}{m_s}(0.0)\frac{w_0}{a^{48}}(0.0)\frac{w_0}{a^{64}}(0.0)\frac{w_0}{a^{96}}(0.0)w_0$
0.2	0.3	0.15	$16.0(0.0)_S(0.0)Z_V^{48}(0.0)Z_V^{64}(0.0)Z_V^{96}(0.2)C_3(1.6)C(0.0)m_l(0.0)\frac{m_l}{m_s}(0.8)\frac{m_p}{m_s}(0.0)\frac{w_0}{a^{48}}(0.0)\frac{w_0}{a^{64}}(0.0)\frac{w_0}{a^{96}}(0.0)w_0$
0.3	0.4	0.15	$20.3(0.0)_S(0.0)Z_V^{48}(0.0)Z_V^{64}(0.0)Z_V^{96}(0.1)C_3(1.1)C(0.0)m_l(0.0)\frac{m_l}{m_s}(0.6)\frac{m_p}{m_s}(0.0)\frac{w_0}{a^{48}}(0.0)\frac{w_0}{a^{64}}(0.0)\frac{w_0}{a^{96}}(0.0)w_0$
0.4	0.5	0.15	$24.65(04)_S(02)Z_V^{48}(05)Z_V^{64}(01)Z_V^{96}(02)C_3(19)C(01)m_l(00)\frac{m_l}{m_s}(08)\frac{m_p}{m_s}(00)\frac{w_0}{a^{48}}(00)\frac{w_0}{a^{64}}(02)w_0$
0.5	0.6	0.15	$29.36(06)_S(03)Z_V^{48}(06)Z_V^{64}(01)Z_V^{96}(03)C_3(27)C(03)m_l(00)\frac{m_l}{m_s}(14)\frac{m_p}{m_s}(00)\frac{w_0}{a^{48}}(00)\frac{w_0}{a^{64}}(01)w_0$
0.6	0.7	0.15	$33.82(10)_S(03)Z_V^{48}(06)Z_V^{64}(01)Z_V^{96}(03)C_3(25)C(04)m_l(00)\frac{m_l}{m_s}(12)\frac{m_p}{m_s}(00)\frac{w_0}{a^{48}}(01)\frac{w_0}{a^{64}}(00)\frac{w_0}{a^{96}}(04)w_0$
0.7	0.8	0.15	$37.28(15)_S(03)Z_V^{48}(07)Z_V^{64}(01)Z_V^{96}(01)C_3(15)C(06)m_l(00)\frac{m_l}{m_s}(05)\frac{m_p}{m_s}(01)\frac{w_0}{a^{48}}(01)\frac{w_0}{a^{64}}(00)\frac{w_0}{a^{96}}(08)w_0$
0.8	0.9	0.15	$39.52(21)_S(03)Z_V^{48}(07)Z_V^{64}(01)Z_V^{96}(01)C_3(01)C(08)m_l(00)\frac{m_l}{m_s}(04)\frac{m_p}{m_s}(01)\frac{w_0}{a^{48}}(02)\frac{w_0}{a^{64}}(00)\frac{w_0}{a^{96}}(13)w_0$
0.9	1.0	0.15	$40.44(28)_S(03)Z_V^{48}(07)Z_V^{64}(02)Z_V^{96}(00)C_3(08)C(10)m_l(00)\frac{m_l}{m_s}(14)\frac{m_p}{m_s}(02)\frac{w_0}{a^{48}}(02)\frac{w_0}{a^{64}}(01)\frac{w_0}{a^{96}}(18)w_0$
1.0	1.1	0.15	$40.57(46)_S(04)Z_V^{48}(10)Z_V^{64}(03)Z_V^{96}(01)C_3(19)C(14)m_l(00)\frac{m_l}{m_s}(12)\frac{m_p}{m_s}(03)\frac{w_0}{a^{48}}(05)\frac{w_0}{a^{64}}(01)\frac{w_0}{a^{96}}(23)w_0$
1.1	1.2	0.15	$39.48(57)_S(04)Z_V^{48}(10)Z_V^{64}(02)Z_V^{96}(01)C_3(21)C(16)m_l(01)\frac{m_l}{m_s}(17)\frac{m_p}{m_s}(04)\frac{w_0}{a^{48}}(06)\frac{w_0}{a^{64}}(01)\frac{w_0}{a^{96}}(27)w_0$
1.2	1.3	0.15	$37.56(68)_S(03)Z_V^{48}(09)Z_V^{64}(01)Z_V^{96}(00)C_3(18)C(18)m_l(01)\frac{m_l}{m_s}(23)\frac{m_p}{m_s}(04)\frac{w_0}{a^{48}}(06)\frac{w_0}{a^{64}}(01)\frac{w_0}{a^{96}}(32)w_0$
1.3	1.4	0.15	$35.00(80)_S(03)Z_V^{48}(07)Z_V^{64}(01)Z_V^{96}(00)C_3(16)C(19)m_l(01)\frac{m_l}{m_s}(27)\frac{m_p}{m_s}(04)\frac{w_0}{a^{48}}(06)\frac{w_0}{a^{64}}(01)\frac{w_0}{a^{96}}(35)w_0$
1.4	1.5	0.15	$31.99(92)_S(02)Z_V^{48}(06)Z_V^{64}(00)C_3(15)C(19)m_l(01)\frac{m_l}{m_s}(27)\frac{m_p}{m_s}(04)\frac{w_0}{a^{48}}(06)\frac{w_0}{a^{64}}(00)\frac{w_0}{a^{96}}(38)w_0$
1.5	1.6	0.15	$28.7(1.0)_S(0.0)Z_V^{48}(0.1)Z_V^{64}(0.0)Z_V^{96}(0.0)C_3(0.1)C(0.2)m_l(0.0)\frac{m_l}{m_s}(0.2)\frac{m_p}{m_s}(0.0)\frac{w_0}{a^{48}}(0.1)\frac{w_0}{a^{64}}(0.0)\frac{w_0}{a^{96}}(0.4)w_0$
1.6	1.7	0.15	$24.65(83)_S(01)Z_V^{48}(02)Z_V^{64}(03)Z_V^{96}(13)C_3(00)C(16)m_l(01)\frac{m_l}{m_s}(43)\frac{m_p}{m_s}(02)\frac{w_0}{a^{48}}(02)\frac{w_0}{a^{64}}(05)\frac{w_0}{a^{96}}(39)w_0$
1.7	1.8	0.15	$21.20(86)_S(01)Z_V^{48}(02)Z_V^{64}(03)Z_V^{96}(10)C_3(01)C(14)m_l(00)\frac{m_l}{m_s}(37)\frac{m_p}{m_s}(02)\frac{w_0}{a^{48}}(02)\frac{w_0}{a^{64}}(05)\frac{w_0}{a^{96}}(37)w_0$
1.8	1.9	0.15	$18.23(88)_S(01)Z_V^{48}(01)Z_V^{64}(03)Z_V^{96}(04)C_3(00)C(13)m_l(00)\frac{m_l}{m_s}(51)\frac{m_p}{m_s}(02)\frac{w_0}{a^{48}}(02)\frac{w_0}{a^{64}}(04)\frac{w_0}{a^{96}}(34)w_0$
1.9	2.0	0.15	$15.57(91)_S(01)Z_V^{48}(01)Z_V^{64}(02)Z_V^{96}(08)C_3(03)C(12)m_l(00)\frac{m_l}{m_s}(61)\frac{m_p}{m_s}(02)\frac{w_0}{a^{48}}(02)\frac{w_0}{a^{64}}(04)\frac{w_0}{a^{96}}(30)w_0$
0.0	0.2	0.15	$16.7(0.0)_S(0.0)Z_V^{48}(0.0)Z_V^{64}(0.0)Z_V^{96}(0.2)C_3(1.3)C(0.0)m_l(0.0)\frac{m_l}{m_s}(0.7)\frac{m_p}{m_s}(0.0)\frac{w_0}{a^{48}}(0.0)\frac{w_0}{a^{64}}(0.0)\frac{w_0}{a^{96}}(0.0)w_0$
0.2	0.4	0.15	$36.3(0.0)_S(0.0)Z_V^{48}(0.1)Z_V^{64}(0.0)Z_V^{96}(0.3)C_3(2.7)C(0.0)m_l(0.0)\frac{m_l}{m_s}(1.4)\frac{m_p}{m_s}(0.0)\frac{w_0}{a^{48}}(0.0)\frac{w_0}{a^{64}}(0.0)\frac{w_0}{a^{96}}(0.0)w_0$
0.4	0.6	0.15	$54.00(10)_S(05)Z_V^{48}(11)Z_V^{64}(01)Z_V^{96}(00)C_3(09)C(04)m_l(00)\frac{m_l}{m_s}(05)\frac{m_p}{m_s}(00)\frac{w_0}{a^{48}}(00)\frac{w_0}{a^{64}}(00)\frac{w_0}{a^{96}}(03)w_0$
0.6	0.8	0.15	$71.11(25)_S(06)Z_V^{48}(14)Z_V^{64}(02)Z_V^{96}(04)C_3(40)C(10)m_l(00)\frac{m_l}{m_s}(17)\frac{m_p}{m_s}(01)\frac{w_0}{a^{48}}(02)\frac{w_0}{a^{64}}(00)\frac{w_0}{a^{96}}(11)w_0$
0.8	1.0	0.15	$79.96(49)_S(06)Z_V^{48}(15)Z_V^{64}(03)Z_V^{96}(01)C_3(07)C(18)m_l(01)\frac{m_l}{m_s}(18)\frac{m_p}{m_s}(03)\frac{w_0}{a^{48}}(04)\frac{w_0}{a^{64}}(01)\frac{w_0}{a^{96}}(31)w_0$
0.3	1.0	0.15	$225.40(85)_S(19)Z_V^{48}(43)Z_V^{64}(08)Z_V^{96}(07)C_3(73)C(34)m_l(01)\frac{m_l}{m_s}(49)\frac{m_p}{m_s}(05)\frac{w_0}{a^{48}}(06)\frac{w_0}{a^{64}}(02)\frac{w_0}{a^{96}}(47)w_0$
0.3	1.3	0.15	$343.3(2.7)_S(0.4)Z_V^{48}(0.9)Z_V^{64}(0.3)Z_V^{96}(0.2)C_3(1.6)C(0.8)m_l(0.0)\frac{m_l}{m_s}(1.1)\frac{m_p}{m_s}(0.2)\frac{w_0}{a^{48}}(0.3)\frac{w_0}{a^{64}}(0.1)\frac{w_0}{a^{96}}(1.3)w_0$
0.3	1.6	0.15	$439.5(5.3)_S(0.4)Z_V^{48}(1.1)Z_V^{64}(0.3)Z_V^{96}(0.2)C_3(2.1)C(1.4)m_l(0.0)\frac{m_l}{m_s}(1.4)\frac{m_p}{m_s}(0.3)\frac{w_0}{a^{48}}(0.5)\frac{w_0}{a^{64}}(0.1)\frac{w_0}{a^{96}}(2.4)w_0$
0.4	1.0	0.15	$205.08(83)_S(17)Z_V^{48}(40)Z_V^{64}(06)Z_V^{96}(05)C_3(42)C(33)m_l(01)\frac{m_l}{m_s}(05)\frac{m_p}{m_s}(05)\frac{w_0}{a^{48}}(07)\frac{w_0}{a^{64}}(01)\frac{w_0}{a^{96}}(45)w_0$
0.4	1.3	0.15	$321.6(2.7)_S(0.3)Z_V^{48}(0.8)Z_V^{64}(0.2)Z_V^{96}(0.1)C_3(0.0)C(0.8)m_l(0.0)\frac{m_l}{m_s}(1.0)\frac{m_p}{m_s}(0.2)\frac{w_0}{a^{48}}(0.3)\frac{w_0}{a^{64}}(0.1)\frac{w_0}{a^{96}}(1.3)w_0$
0.4	1.6	0.15	$418.3(5.3)_S(0.4)Z_V^{48}(1.0)Z_V^{64}(0.2)Z_V^{96}(0.0)C_3(0.5)C(1.4)m_l(0.0)\frac{m_l}{m_s}(1.3)\frac{m_p}{m_s}(0.3)\frac{w_0}{a^{48}}(0.5)\frac{w_0}{a^{64}}(0.1)\frac{w_0}{a^{96}}(2.4)w_0$
0.4	1.0	0.05	$208.4(0.8)_S(0.2)Z_V^{48}(0.4)Z_V^{64}(0.1)Z_V^{96}(0.1)C_3(1.2)C(0.3)m_l(0.0)\frac{m_l}{m_s}(0.6)\frac{m_p}{m_s}(0.0)\frac{w_0}{a^{48}}(0.1)\frac{w_0}{a^{64}}(0.0)\frac{w_0}{a^{96}}(0.7)w_0$
0.4	1.0	0.1	$207.4(0.8)_S(0.2)Z_V^{48}(0.4)Z_V^{64}(0.1)Z_V^{96}(0.1)C_3(1.0)C(0.3)m_l(0.0)\frac{m_l}{m_s}(0.4)\frac{m_p}{m_s}(0.0)\frac{w_0}{a^{48}}(0.1)\frac{w_0}{a^{64}}(0.0)\frac{w_0}{a^{96}}(0.4)w_0$
0.4	1.0	0.2	$201.83(86)_S(17)Z_V^{48}(38)Z_V^{64}(07)Z_V^{96}(01)C_3(05)C(33)m_l(01)\frac{m_l}{m_s}(22)\frac{m_p}{m_s}(05)\frac{w_0}{a^{48}}(07)\frac{w_0}{a^{64}}(02)\frac{w_0}{a^{96}}(48)w_0$

TABLE XIV. Same as Table X, but for the strange quark mass data.

t_0/fm	t_1/fm	Δ/fm	$a_\mu^{\text{s,conn.isospin,W}} \times 10^{10}$
Total			$52.83(22)_S(04)_{Z_V^{64}}(20)_{Z_V^{96}}(30)_{C_3}(03)_{\frac{w_0}{a^{64}}(13)}_{\frac{w_0}{a^{96}}(53)}_{w_0}$
0.0	0.1	0.15	$0.81(00)_S(00)_{Z_V^{64}}(00)_{Z_V^{96}}(12)_{C_3}(00)_{\frac{w_0}{a^{64}}(00)}_{\frac{w_0}{a^{96}}(00)}_{w_0}$
0.1	0.2	0.15	$1.666(01)_S(01)_{Z_V^{64}}(06)_{Z_V^{96}}(10)_{C_3}(00)_{\frac{w_0}{a^{64}}(00)}_{\frac{w_0}{a^{96}}(01)}_{w_0}$
0.2	0.3	0.15	$2.57(00)_S(00)_{Z_V^{64}}(01)_{Z_V^{96}}(16)_{C_3}(00)_{\frac{w_0}{a^{64}}(00)}_{\frac{w_0}{a^{96}}(00)}_{w_0}$
0.3	0.4	0.15	$3.448(05)_S(02)_{Z_V^{64}}(13)_{Z_V^{96}}(63)_{C_3}(00)_{\frac{w_0}{a^{64}}(01)}_{\frac{w_0}{a^{96}}(04)}_{w_0}$
0.4	0.5	0.15	$4.170(07)_S(03)_{Z_V^{64}}(16)_{Z_V^{96}}(08)_{C_3}(00)_{\frac{w_0}{a^{64}}(02)}_{\frac{w_0}{a^{96}}(08)}_{w_0}$
0.5	0.6	0.15	$4.666(10)_S(03)_{Z_V^{64}}(18)_{Z_V^{96}}(53)_{C_3}(01)_{\frac{w_0}{a^{64}}(04)}_{\frac{w_0}{a^{96}}(16)}_{w_0}$
0.6	0.7	0.15	$4.866(13)_S(04)_{Z_V^{64}}(18)_{Z_V^{96}}(67)_{C_3}(01)_{\frac{w_0}{a^{64}}(06)}_{\frac{w_0}{a^{96}}(24)}_{w_0}$
0.7	0.8	0.15	$4.799(16)_S(03)_{Z_V^{64}}(18)_{Z_V^{96}}(08)_{C_3}(02)_{\frac{w_0}{a^{64}}(08)}_{\frac{w_0}{a^{96}}(33)}_{w_0}$
0.8	0.9	0.15	$4.505(17)_S(03)_{Z_V^{64}}(17)_{Z_V^{96}}(03)_{C_3}(02)_{\frac{w_0}{a^{64}}(10)}_{\frac{w_0}{a^{96}}(39)}_{w_0}$
0.9	1.0	0.15	$4.058(19)_S(03)_{Z_V^{64}}(15)_{Z_V^{96}}(43)_{C_3}(02)_{\frac{w_0}{a^{64}}(11)}_{\frac{w_0}{a^{96}}(45)}_{w_0}$
1.0	1.1	0.15	$3.527(19)_S(03)_{Z_V^{64}}(13)_{Z_V^{96}}(57)_{C_3}(02)_{\frac{w_0}{a^{64}}(12)}_{\frac{w_0}{a^{96}}(46)}_{w_0}$
1.1	1.2	0.15	$2.973(19)_S(02)_{Z_V^{64}}(11)_{Z_V^{96}}(57)_{C_3}(02)_{\frac{w_0}{a^{64}}(12)}_{\frac{w_0}{a^{96}}(46)}_{w_0}$
1.2	1.3	0.15	$2.441(18)_S(02)_{Z_V^{64}}(09)_{Z_V^{96}}(62)_{C_3}(02)_{\frac{w_0}{a^{64}}(11)}_{\frac{w_0}{a^{96}}(44)}_{w_0}$
1.3	1.4	0.15	$1.955(17)_S(01)_{Z_V^{64}}(07)_{Z_V^{96}}(52)_{C_3}(02)_{\frac{w_0}{a^{64}}(10)}_{\frac{w_0}{a^{96}}(40)}_{w_0}$
1.4	1.5	0.15	$1.534(15)_S(01)_{Z_V^{64}}(06)_{Z_V^{96}}(47)_{C_3}(02)_{\frac{w_0}{a^{64}}(09)}_{\frac{w_0}{a^{96}}(35)}_{w_0}$
1.5	1.6	0.15	$1.181(13)_S(01)_{Z_V^{64}}(05)_{Z_V^{96}}(41)_{C_3}(01)_{\frac{w_0}{a^{64}}(08)}_{\frac{w_0}{a^{96}}(30)}_{w_0}$
1.6	1.7	0.15	$0.894(12)_S(01)_{Z_V^{64}}(03)_{Z_V^{96}}(35)_{C_3}(01)_{\frac{w_0}{a^{64}}(06)}_{\frac{w_0}{a^{96}}(25)}_{w_0}$
1.7	1.8	0.15	$0.667(10)_S(00)_{Z_V^{64}}(03)_{Z_V^{96}}(30)_{C_3}(01)_{\frac{w_0}{a^{64}}(05)}_{\frac{w_0}{a^{96}}(21)}_{w_0}$
1.8	1.9	0.15	$0.491(08)_S(00)_{Z_V^{64}}(02)_{Z_V^{96}}(25)_{C_3}(01)_{\frac{w_0}{a^{64}}(04)}_{\frac{w_0}{a^{96}}(17)}_{w_0}$
1.9	2.0	0.15	$0.357(07)_S(00)_{Z_V^{64}}(01)_{Z_V^{96}}(20)_{C_3}(01)_{\frac{w_0}{a^{64}}(03)}_{\frac{w_0}{a^{96}}(13)}_{w_0}$
0.0	0.2	0.15	$2.48(00)_S(00)_{Z_V^{64}}(01)_{Z_V^{96}}(11)_{C_3}(00)_{\frac{w_0}{a^{64}}(00)}_{\frac{w_0}{a^{96}}(00)}_{w_0}$
0.2	0.4	0.15	$6.02(01)_S(00)_{Z_V^{64}}(02)_{Z_V^{96}}(10)_{C_3}(00)_{\frac{w_0}{a^{64}}(00)}_{\frac{w_0}{a^{96}}(01)}_{w_0}$
0.4	0.6	0.15	$8.837(18)_S(06)_{Z_V^{64}}(34)_{Z_V^{96}}(61)_{C_3}(01)_{\frac{w_0}{a^{64}}(06)}_{\frac{w_0}{a^{96}}(24)}_{w_0}$
0.6	0.8	0.15	$9.666(29)_S(07)_{Z_V^{64}}(37)_{Z_V^{96}}(59)_{C_3}(03)_{\frac{w_0}{a^{64}}(14)}_{\frac{w_0}{a^{96}}(57)}_{w_0}$
0.8	1.0	0.15	$8.562(36)_S(06)_{Z_V^{64}}(33)_{Z_V^{96}}(45)_{C_3}(04)_{\frac{w_0}{a^{64}}(21)}_{\frac{w_0}{a^{96}}(84)}_{w_0}$
0.3	1.0	0.15	$30.51(08)_S(02)_{Z_V^{64}}(12)_{Z_V^{96}}(14)_{C_3}(01)_{\frac{w_0}{a^{64}}(04)}_{\frac{w_0}{a^{96}}(17)}_{w_0}$
0.3	1.3	0.15	$39.45(13)_S(03)_{Z_V^{64}}(15)_{Z_V^{96}}(04)_{C_3}(01)_{\frac{w_0}{a^{64}}(08)}_{\frac{w_0}{a^{96}}(31)}_{w_0}$
0.3	1.6	0.15	$44.12(17)_S(03)_{Z_V^{64}}(17)_{Z_V^{96}}(18)_{C_3}(02)_{\frac{w_0}{a^{64}}(10)}_{\frac{w_0}{a^{96}}(41)}_{w_0}$
0.4	1.0	0.15	$27.06(08)_S(02)_{Z_V^{64}}(10)_{Z_V^{96}}(08)_{C_3}(01)_{\frac{w_0}{a^{64}}(04)}_{\frac{w_0}{a^{96}}(16)}_{w_0}$
0.4	1.3	0.15	$36.01(13)_S(03)_{Z_V^{64}}(14)_{Z_V^{96}}(10)_{C_3}(01)_{\frac{w_0}{a^{64}}(08)}_{\frac{w_0}{a^{96}}(30)}_{w_0}$
0.4	1.6	0.15	$40.68(17)_S(03)_{Z_V^{64}}(15)_{Z_V^{96}}(24)_{C_3}(02)_{\frac{w_0}{a^{64}}(10)}_{\frac{w_0}{a^{96}}(41)}_{w_0}$
0.4	1.0	0.05	$27.9(0.1)_S(0.0)_{Z_V^{64}}(0.1)_{Z_V^{96}}(1.1)_{C_3}(0.0)_{\frac{w_0}{a^{64}}(0.0)}_{\frac{w_0}{a^{96}}(0.2)}_{w_0}$
0.4	1.0	0.1	$27.70(08)_S(02)_{Z_V^{64}}(11)_{Z_V^{96}}(05)_{C_3}(01)_{\frac{w_0}{a^{64}}(04)}_{\frac{w_0}{a^{96}}(17)}_{w_0}$
0.4	1.0	0.2	$26.24(08)_S(02)_{Z_V^{64}}(10)_{Z_V^{96}}(06)_{C_3}(01)_{\frac{w_0}{a^{64}}(04)}_{\frac{w_0}{a^{96}}(16)}_{w_0}$

TABLE XV. Same as Table XIV, but for the p prescription.

t_0/fm	t_1/fm	Δ/fm	$a_\mu^{\text{s,conn,isospin,W}} \times 10^{10}$
Total			$53.08(22)_S(04)_{Z_V^{64}}(20)_{Z_V^{96}}(58)_{C_3}(03)_{\frac{w_0}{a^{64}}(13)}_{\frac{w_0}{a^{96}}(53)}_{w_0}$
0.0	0.1	0.15	$0.887(00)_S(01)_{Z_V^{64}}(03)_{Z_V^{96}}(40)_{C_3}(00)_{\frac{w_0}{a^{64}}(00)}_{\frac{w_0}{a^{96}}(00)}_{w_0}$
0.1	0.2	0.15	$1.728(01)_S(01)_{Z_V^{64}}(06)_{Z_V^{96}}(86)_{C_3}(00)_{\frac{w_0}{a^{64}}(00)}_{\frac{w_0}{a^{96}}(02)}_{w_0}$
0.2	0.3	0.15	$2.59(00)_S(00)_{Z_V^{64}}(01)_{Z_V^{96}}(24)_{C_3}(00)_{\frac{w_0}{a^{64}}(00)}_{\frac{w_0}{a^{96}}(00)}_{w_0}$
0.3	0.4	0.15	$3.451(05)_S(03)_{Z_V^{64}}(13)_{Z_V^{96}}(47)_{C_3}(00)_{\frac{w_0}{a^{64}}(01)}_{\frac{w_0}{a^{96}}(04)}_{w_0}$
0.4	0.5	0.15	$4.169(08)_S(03)_{Z_V^{64}}(16)_{Z_V^{96}}(15)_{C_3}(00)_{\frac{w_0}{a^{64}}(02)}_{\frac{w_0}{a^{96}}(08)}_{w_0}$
0.5	0.6	0.15	$4.665(11)_S(03)_{Z_V^{64}}(18)_{Z_V^{96}}(59)_{C_3}(01)_{\frac{w_0}{a^{64}}(04)}_{\frac{w_0}{a^{96}}(16)}_{w_0}$
0.6	0.7	0.15	$4.866(13)_S(04)_{Z_V^{64}}(19)_{Z_V^{96}}(73)_{C_3}(01)_{\frac{w_0}{a^{64}}(06)}_{\frac{w_0}{a^{96}}(24)}_{w_0}$
0.7	0.8	0.15	$4.799(16)_S(04)_{Z_V^{64}}(18)_{Z_V^{96}}(06)_{C_3}(02)_{\frac{w_0}{a^{64}}(08)}_{\frac{w_0}{a^{96}}(33)}_{w_0}$
0.8	0.9	0.15	$4.504(18)_S(03)_{Z_V^{64}}(17)_{Z_V^{96}}(02)_{C_3}(02)_{\frac{w_0}{a^{64}}(10)}_{\frac{w_0}{a^{96}}(39)}_{w_0}$
0.9	1.0	0.15	$4.058(19)_S(03)_{Z_V^{64}}(16)_{Z_V^{96}}(43)_{C_3}(02)_{\frac{w_0}{a^{64}}(11)}_{\frac{w_0}{a^{96}}(45)}_{w_0}$
1.0	1.1	0.15	$3.527(19)_S(03)_{Z_V^{64}}(14)_{Z_V^{96}}(58)_{C_3}(02)_{\frac{w_0}{a^{64}}(12)}_{\frac{w_0}{a^{96}}(46)}_{w_0}$
1.1	1.2	0.15	$2.973(19)_S(02)_{Z_V^{64}}(11)_{Z_V^{96}}(57)_{C_3}(02)_{\frac{w_0}{a^{64}}(12)}_{\frac{w_0}{a^{96}}(46)}_{w_0}$
1.2	1.3	0.15	$2.440(18)_S(02)_{Z_V^{64}}(09)_{Z_V^{96}}(62)_{C_3}(02)_{\frac{w_0}{a^{64}}(11)}_{\frac{w_0}{a^{96}}(44)}_{w_0}$
1.3	1.4	0.15	$1.955(17)_S(01)_{Z_V^{64}}(08)_{Z_V^{96}}(52)_{C_3}(02)_{\frac{w_0}{a^{64}}(10)}_{\frac{w_0}{a^{96}}(40)}_{w_0}$
1.4	1.5	0.15	$1.534(15)_S(01)_{Z_V^{64}}(06)_{Z_V^{96}}(47)_{C_3}(02)_{\frac{w_0}{a^{64}}(09)}_{\frac{w_0}{a^{96}}(35)}_{w_0}$
1.5	1.6	0.15	$1.181(13)_S(01)_{Z_V^{64}}(05)_{Z_V^{96}}(41)_{C_3}(01)_{\frac{w_0}{a^{64}}(08)}_{\frac{w_0}{a^{96}}(30)}_{w_0}$
1.6	1.7	0.15	$0.894(12)_S(01)_{Z_V^{64}}(03)_{Z_V^{96}}(35)_{C_3}(01)_{\frac{w_0}{a^{64}}(06)}_{\frac{w_0}{a^{96}}(25)}_{w_0}$
1.7	1.8	0.15	$0.667(10)_S(00)_{Z_V^{64}}(03)_{Z_V^{96}}(31)_{C_3}(01)_{\frac{w_0}{a^{64}}(05)}_{\frac{w_0}{a^{96}}(21)}_{w_0}$
1.8	1.9	0.15	$0.491(08)_S(00)_{Z_V^{64}}(02)_{Z_V^{96}}(25)_{C_3}(01)_{\frac{w_0}{a^{64}}(04)}_{\frac{w_0}{a^{96}}(17)}_{w_0}$
1.9	2.0	0.15	$0.357(07)_S(00)_{Z_V^{64}}(01)_{Z_V^{96}}(21)_{C_3}(01)_{\frac{w_0}{a^{64}}(03)}_{\frac{w_0}{a^{96}}(13)}_{w_0}$
0.0	0.2	0.15	$2.615(02)_S(02)_{Z_V^{64}}(10)_{Z_V^{96}}(46)_{C_3}(00)_{\frac{w_0}{a^{64}}(00)}_{\frac{w_0}{a^{96}}(02)}_{w_0}$
0.2	0.4	0.15	$6.05(01)_S(00)_{Z_V^{64}}(02)_{Z_V^{96}}(19)_{C_3}(00)_{\frac{w_0}{a^{64}}(00)}_{\frac{w_0}{a^{96}}(01)}_{w_0}$
0.4	0.6	0.15	$8.834(18)_S(07)_{Z_V^{64}}(34)_{Z_V^{96}}(74)_{C_3}(01)_{\frac{w_0}{a^{64}}(06)}_{\frac{w_0}{a^{96}}(24)}_{w_0}$
0.6	0.8	0.15	$9.665(29)_S(07)_{Z_V^{64}}(37)_{Z_V^{96}}(67)_{C_3}(03)_{\frac{w_0}{a^{64}}(14)}_{\frac{w_0}{a^{96}}(57)}_{w_0}$
0.8	1.0	0.15	$8.562(36)_S(06)_{Z_V^{64}}(33)_{Z_V^{96}}(44)_{C_3}(04)_{\frac{w_0}{a^{64}}(21)}_{\frac{w_0}{a^{96}}(84)}_{w_0}$
0.3	1.0	0.15	$30.51(09)_S(02)_{Z_V^{64}}(12)_{Z_V^{96}}(14)_{C_3}(01)_{\frac{w_0}{a^{64}}(04)}_{\frac{w_0}{a^{96}}(17)}_{w_0}$
0.3	1.3	0.15	$39.45(13)_S(03)_{Z_V^{64}}(15)_{Z_V^{96}}(03)_{C_3}(02)_{\frac{w_0}{a^{64}}(08)}_{\frac{w_0}{a^{96}}(31)}_{w_0}$
0.3	1.6	0.15	$44.12(17)_S(03)_{Z_V^{64}}(17)_{Z_V^{96}}(17)_{C_3}(02)_{\frac{w_0}{a^{64}}(10)}_{\frac{w_0}{a^{96}}(41)}_{w_0}$
0.4	1.0	0.15	$27.06(08)_S(02)_{Z_V^{64}}(10)_{Z_V^{96}}(10)_{C_3}(01)_{\frac{w_0}{a^{64}}(04)}_{\frac{w_0}{a^{96}}(16)}_{w_0}$
0.4	1.3	0.15	$36.00(13)_S(03)_{Z_V^{64}}(14)_{Z_V^{96}}(08)_{C_3}(01)_{\frac{w_0}{a^{64}}(08)}_{\frac{w_0}{a^{96}}(30)}_{w_0}$
0.4	1.6	0.15	$40.67(17)_S(03)_{Z_V^{64}}(16)_{Z_V^{96}}(22)_{C_3}(02)_{\frac{w_0}{a^{64}}(10)}_{\frac{w_0}{a^{96}}(41)}_{w_0}$
0.4	1.0	0.05	$27.9(0.1)_S(0.0)_{Z_V^{64}}(0.1)_{Z_V^{96}}(1.1)_{C_3}(0.0)_{\frac{w_0}{a^{64}}(0.0)}_{\frac{w_0}{a^{96}}(0.2)}_{w_0}$
0.4	1.0	0.1	$27.69(08)_S(02)_{Z_V^{64}}(11)_{Z_V^{96}}(03)_{C_3}(01)_{\frac{w_0}{a^{64}}(04)}_{\frac{w_0}{a^{96}}(17)}_{w_0}$
0.4	1.0	0.2	$26.24(08)_S(02)_{Z_V^{64}}(10)_{Z_V^{96}}(07)_{C_3}(01)_{\frac{w_0}{a^{64}}(04)}_{\frac{w_0}{a^{96}}(16)}_{w_0}$

- [1] M. Davier, A. Hoecker, B. Malaescu, and Z. Zhang, A new evaluation of the hadronic vacuum polarisation contributions to the muon anomalous magnetic moment and to $\alpha(m_Z^2)$, *Eur. Phys. J. C* **80**, 241 (2020).
- [2] A. Keshavarzi, D. Nomura, and T. Teubner, $g - 2$ of charged leptons, $\alpha(M_Z^2)$, and the hyperfine splitting of muonium, *Phys. Rev. D* **101**, 014029 (2020).
- [3] G. W. Bennett *et al.* (Muon g-2 Collaboration), Final report of the Muon E821 anomalous magnetic moment measurement at BNL, *Phys. Rev. D* **73**, 072003 (2006).
- [4] J. Grange *et al.* (Muon g-2 Collaboration), Muon (g-2) technical design report, [arXiv:1501.06858](https://arxiv.org/abs/1501.06858).
- [5] M. Abe *et al.*, A new approach for measuring the Muon anomalous magnetic moment and electric dipole moment, *Prog. Theor. Exp. Phys.* **2019**, 053C02 (2019).
- [6] K. Hagiwara, R. Liao, A. D. Martin, D. Nomura, and T. Teubner, $(g - 2)_\mu$ and $\alpha(M_Z^2)$ re-evaluated using new precise data, *J. Phys. G* **38**, 085003 (2011).
- [7] M. Davier, A. Hoecker, B. Malaescu, and Z. Zhang, Reevaluation of the Hadronic contributions to the muon $g - 2$ and to $\alpha(M_Z)$, *Eur. Phys. J. C* **71**, 1515 (2011); Erratum, *Eur. Phys. J. C* **72**, 1874(E) (2012).
- [8] M. Davier, A. Hoecker, B. Malaescu, and Z. Zhang, Reevaluation of the hadronic vacuum polarisation contributions to the Standard Model predictions of the muon $g - 2$ and $\alpha(m_Z^2)$ using newest hadronic cross-section data, *Eur. Phys. J. C* **77**, 827 (2017).
- [9] F. Jegerlehner, Muon g-2 theory: The hadronic part, *EPJ Web Conf.* **166**, 00022 (2018).
- [10] A. Keshavarzi, D. Nomura, and T. Teubner, Muon g-2 and $\alpha(M_Z^2)$: A new data-based analysis, *Phys. Rev. D* **97**, 114025 (2018).
- [11] F. Burger, X. Feng, G. Hotzel, K. Jansen, M. Petschlies, and D. B. Renner (ETM Collaboration), Four-flavour leading-order Hadronic contribution to the muon anomalous magnetic moment, *J. High Energy Phys.* **02** (2014) 099.
- [12] T. Blum, P. A. Boyle, T. Izubuchi, L. Jin, A. Jüttner, C. Lehner, K. Maltman, M. Marinkovic, A. Portelli, and M. Spraggs, Calculation of the Hadronic Vacuum Polarization Disconnected Contribution to the Muon Anomalous Magnetic Moment, *Phys. Rev. Lett.* **116**, 232002 (2016).
- [13] T. Blum *et al.* (RBC/UKQCD Collaboration), Lattice calculation of the leading strange quark-connected contribution to the muon $g - 2$, *J. High Energy Phys.* **04** (2016) 063; Erratum, *J. High Energy Phys.* **05** (2017) 034.
- [14] B. Chakraborty, C. T. H. Davies, P. G. de Oliveira, J. Koponen, G. P. Lepage, and R. S. Van de Water, The hadronic vacuum polarization contribution to a_μ from full lattice QCD, *Phys. Rev. D* **96**, 034516 (2017).
- [15] M. A. Clark, C. Jung, and C. Lehner, Multi-Grid Lanczos, *EPJ Web Conf.* **175**, 14023 (2018).
- [16] C. Lehner (RBC and UKQCD Collaborations), A precise determination of the HVP contribution to the muon anomalous magnetic moment from lattice QCD, *EPJ Web Conf.* **175**, 01024 (2018).
- [17] B. Chakraborty *et al.* (Fermilab Lattice, LATTICE-HPQCD, and MILC Collaborations), Strong-Isospin-Breaking Correction to the Muon Anomalous Magnetic Moment from Lattice QCD at the Physical Point, *Phys. Rev. Lett.* **120**, 152001 (2018).
- [18] P. Boyle, V. Gülpers, J. Harrison, A. Jüttner, C. Lehner, A. Portelli, and C. T. Sachrajda, Isospin breaking corrections to meson masses and the hadronic vacuum polarization: A comparative study, *J. High Energy Phys.* **09** (2017) 153.
- [19] M. Della Morte, A. Francis, V. Gülpers, G. Herdoza, G. von Hippel, H. Horch, B. Jger, H. B. Meyer, A. Nyffeler, and H. Wittig, The hadronic vacuum polarization contribution to the muon $g - 2$ from lattice QCD, *J. High Energy Phys.* **10** (2017) 020.
- [20] S. Borsanyi *et al.* (Budapest-Marseille-Wuppertal Collaboration), Hadronic Vacuum Polarization Contribution to the Anomalous Magnetic Moments of Leptons from First Principles, *Phys. Rev. Lett.* **121**, 022002 (2018).
- [21] T. Blum, P. A. Boyle, V. Gülpers, T. Izubuchi, L. Jin, C. Jung, A. Jüttner, C. Lehner, A. Portelli, and J. T. Tsang (RBC and UKQCD Collaborations), Calculation of the Hadronic Vacuum Polarization Contribution to the Muon Anomalous Magnetic Moment, *Phys. Rev. Lett.* **121**, 022003 (2018).
- [22] D. Giusti, F. Sanfilippo, and S. Simula, Light-quark contribution to the leading hadronic vacuum polarization term of the muon $g - 2$ from twisted-mass fermions, *Phys. Rev. D* **98**, 114504 (2018).
- [23] T. Izubuchi, Y. Kuramashi, C. Lehner, and E. Shintani (PACS Collaboration), Finite-volume correction on the hadronic vacuum polarization contribution to the muon $g - 2$ in lattice QCD, *Phys. Rev. D* **98**, 054505 (2018).
- [24] C. T. H. Davies *et al.* (Fermilab Lattice, LATTICE-HPQCD, and MILC Collaborations), Hadronic-vacuum-polarization contribution to the muons anomalous magnetic moment from four-flavor lattice QCD, *Phys. Rev. D* **101**, 034512 (2020).
- [25] E. Shintani and Y. Kuramashi (PACS Collaboration), Hadronic vacuum polarization contribution to the muon $g - 2$ with $2 + 1$ flavor lattice QCD on a larger than $(10 \text{ fm})^4$ lattice at the physical point, *Phys. Rev. D* **100**, 034517 (2019).
- [26] A. Gérardin, M. Cè, G. von Hippel, B. Hörrz, H. B. Meyer, D. Mohler, K. Ottnad, J. Wilhelm, and H. Wittig, The leading hadronic contribution to $(g - 2)_\mu$ from lattice QCD with $N_f = 2 + 1$ flavours of O(a) improved Wilson quarks, *Phys. Rev. D* **100**, 014510 (2019).
- [27] S. Borsanyi *et al.*, Leading-order hadronic vacuum polarization contribution to the muon magnetic moment from lattice QCD, [arXiv:2002.12347](https://arxiv.org/abs/2002.12347).
- [28] C. Lehner *et al.* (USQCD Collaboration), Opportunities for lattice QCD in quark and lepton flavor physics, *Eur. Phys. J. A* **55**, 195 (2019).
- [29] D. Giusti, V. Lubicz, G. Martinelli, F. Sanfilippo, and S. Simula, Electromagnetic and strong isospin-breaking corrections to the muon $g - 2$ from Lattice QCD + QED, *Phys. Rev. D* **99**, 114502 (2019).
- [30] D. Giusti and S. Simula, Lepton anomalous magnetic moments in Lattice QCD + QED, Proc. Sci., LATTICE2019 (2019) 104 [[arXiv:1910.03874](https://arxiv.org/abs/1910.03874)].
- [31] J. Prades, E. de Rafael, and A. Vainshtein, The Hadronic light-by-light scattering contribution to the Muon and electron anomalous magnetic moments, *Adv. Ser. Dir. High Energy Phys.* **20**, 303 (2009).

- [32] T. Blum, N. Christ, M. Hayakawa, T. Izubuchi, L. Jin, C. Jung, and C. Lehner, Hadronic light-by-light contribution to the muon anomalous magnetic moment from lattice QCD, in *54th Rencontres de Moriond on Electroweak Interactions and Unified Theories (Moriond EW 2019) La Thuile, Italy* (2019).
- [33] First plenary workshop of the muon g-2 theory initiative, <https://indico.fnal.gov/event/13795/> (2017).
- [34] Workshop on hadronic vacuum polarization contributions to muon g-2, <https://kds.kek.jp/indico/event/26780/> (2018).
- [35] Muon g-2 theory initiative hadronic light-by-light working group workshop, <https://indico.phys.uconn.edu/event/1/> (2018).
- [36] Second plenary workshop of the muon g-2 theory initiative, <https://indico.him.uni-mainz.de/event/11/overview> (2018).
- [37] Third plenary workshop of the muon g-2 theory initiative, <https://indico.fnal.gov/event/21626/overview> (2019).
- [38] Muon g-2 theory initiative, Muon g-2 theory initiative white paper (to be published).
- [39] G. Colangelo, M. Hoferichter, M. Procura, and P. Stoffer, Dispersion relation for hadronic light-by-light scattering: Theoretical foundations, *J. High Energy Phys.* **09** (2015) 074.
- [40] G. Colangelo, M. Hoferichter, M. Procura, and P. Stoffer, Dispersion relation for hadronic light-by-light scattering: Two-pion contributions, *J. High Energy Phys.* **04** (2017) 161.
- [41] G. Colangelo, M. Hoferichter, M. Procura, and P. Stoffer, Rescattering Effects in the Hadronic-Light-by-Light Contribution to the Anomalous Magnetic Moment of the Muon, *Phys. Rev. Lett.* **118**, 232001 (2017).
- [42] G. Colangelo, F. Hagelstein, M. Hoferichter, L. Laub, and P. Stoffer, Longitudinal short-distance constraints for the hadronic light-by-light contribution to $(g-2)_\mu$ with large- N_c Regge models, *J. High Energy Phys.* **03** (2020) 101.
- [43] G. Colangelo, F. Hagelstein, M. Hoferichter, L. Laub, and P. Stoffer, Short-distance constraints on hadronic light-by-light scattering in the anomalous magnetic moment of the muon, *Phys. Rev. D* **101**, 051501 (2020).
- [44] T. Blum, S. Chowdhury, M. Hayakawa, and T. Izubuchi, Hadronic Light-by-Light Scattering Contribution to the Muon Anomalous Magnetic Moment from Lattice QCD, *Phys. Rev. Lett.* **114**, 012001 (2015).
- [45] T. Blum, N. Christ, M. Hayakawa, T. Izubuchi, L. Jin, and C. Lehner, Lattice calculation of hadronic light-by-light contribution to the Muon anomalous magnetic moment, *Phys. Rev. D* **93**, 014503 (2016).
- [46] T. Blum, N. Christ, M. Hayakawa, T. Izubuchi, L. Jin, C. Jung, and C. Lehner, Connected and Leading Disconnected Hadronic Light-by-Light Contribution to the Muon Anomalous Magnetic Moment with a Physical Pion Mass, *Phys. Rev. Lett.* **118**, 022005 (2017).
- [47] T. Blum, N. Christ, M. Hayakawa, T. Izubuchi, L. Jin, C. Jung, and C. Lehner, Using infinite volume, continuum QED and lattice QCD for the hadronic light-by-light contribution to the muon anomalous magnetic moment, *Phys. Rev. D* **96**, 034515 (2017).
- [48] N. Asmussen, J. Green, H. B. Meyer, and A. Nyffeler, Position-space approach to hadronic light-by-light scattering in the muon $g-2$ on the lattice, *Proc. Sci., LATTICE2016* (2016) 164.
- [49] J. Green, O. Gryniuk, G. von Hippel, H. B. Meyer, and V. Pascalutsa, Lattice QCD Calculation of Hadronic Light-by-Light Scattering, *Phys. Rev. Lett.* **115**, 222003 (2015).
- [50] C. Aubin, T. Blum, C. Tu, M. Golterman, C. Jung, and S. Peris, Light quark vacuum polarization at the physical point and contribution to the muon $g-2$, *Phys. Rev. D* **101**, 014503 (2020).
- [51] D. Bernecker and H. B. Meyer, Vector correlators in lattice QCD: Methods and applications, *Eur. Phys. J. A* **47**, 148 (2011).
- [52] S. Aoki *et al.* (Flavour Lattice Averaging Group), FLAG review 2019, *Eur. Phys. J. C* **80**, 113 (2020).
- [53] C. Lehner and T. Izubuchi, Towards the large volume limit—A method for lattice QCD + QED simulations, *Proc. Sci., LATTICE2014* (2015) 164 [arXiv:1503.04395].
- [54] J. A. Bailey *et al.*, The $B \rightarrow \pi \ell \nu$ semileptonic form factor from three-flavor lattice QCD: A model-independent determination of $|V_{ub}|$, *Phys. Rev. D* **79**, 054507 (2009).
- [55] M. Tanabashi *et al.* (Particle Data Group), Review of particle physics, *Phys. Rev. D* **98**, 030001 (2018).
- [56] A. Bazavov *et al.* (Fermilab Lattice and MILC Collaborations), Charmed and light pseudoscalar meson decay constants from four-flavor Lattice QCD with physical light quarks, *Phys. Rev. D* **90**, 074509 (2014).
- [57] R. J. Dowdall, C. T. H. Davies, G. P. Lepage, and C. McNeile, V_{us} from π and K decay constants in full lattice QCD with physical u, d, s and c quarks, *Phys. Rev. D* **88**, 074504 (2013).
- [58] S. Collins, G. Bali, and A. Schafer, Disconnected contributions to hadronic structure: A new method for stochastic noise reduction, *Proc. Sci., LATTICE2007* (2007) 141 [arXiv:0709.3217].
- [59] E. Shintani, R. Arthur, T. Blum, T. Izubuchi, C. Jung, and C. Lehner, Covariant approximation averaging, *Phys. Rev. D* **91**, 114511 (2015).
- [60] C. Lehner, The hadronic vacuum polarization contribution to the muon anomalous magnetic moment, RBRC Workshop on Lattice Gauge Theories (2016).
- [61] G. J. Gounaris and J. J. Sakurai, Finite Width Corrections to the Vector Meson Dominance Prediction for $\rho \rightarrow e^+ e^-$, *Phys. Rev. Lett.* **21**, 244 (1968).
- [62] M. Lüscher, Two particle states on a torus and their relation to the scattering matrix, *Nucl. Phys.* **B354**, 531 (1991).
- [63] L. Lellouch and M. Lüscher, Weak transition matrix elements from finite volume correlation functions, *Commun. Math. Phys.* **219**, 31 (2001).
- [64] H. B. Meyer, Lattice QCD and the Timelike Pion Form Factor, *Phys. Rev. Lett.* **107**, 072002 (2011).
- [65] M. Della Morte and A. Juttner, Quark disconnected diagrams in chiral perturbation theory, *J. High Energy Phys.* **11** (2010) 154.
- [66] Aubin *et al.* (private communication), 2020.